

Synthetic Strategies for Improving Solubility: Optimization of Novel Pyrazolo[1,5-*a*]pyrimidine CFTR Activator That Ameliorates Dry Eye Disease

Bo Yi Kim, Changmok Oh, Dongkyu Jeon, Ikhyun Jun, Ho K. Lee, Bo-Rahm Kim, Jinhong Park, Kyoung Yul Seo, Kyeong-A Kim, Dami Lim, Seolhee Lee, Jooyun Lee, Hongchul Yoon,* Tae-im Kim,* and Wan Namkung*

Cite This: *J. Med. Chem.* 2023, 66, 413–434

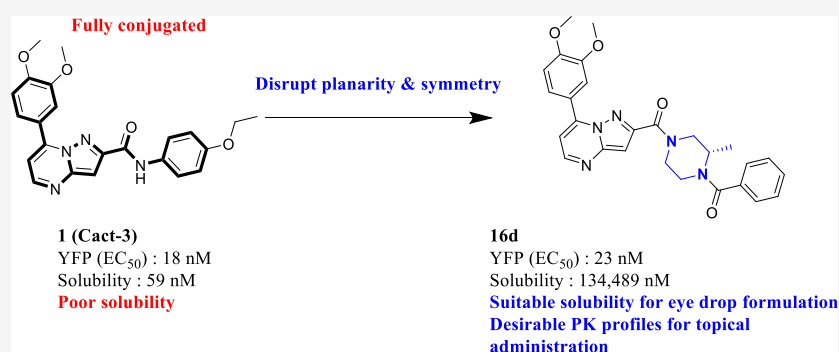
Read Online

ACCESS |

Metrics & More

Article Recommendations

Supporting Information



ABSTRACT: Dry eye disease (DED) is one of the most prevalent ocular diseases but has limited treatment options. Cystic fibrosis transmembrane conductance regulator (CFTR), a major chloride channel that stimulates fluid secretion in the ocular surface, may pave the way for new therapeutic strategies for DED. Herein, we report the optimization of Cact-3, a potent CFTR activator with poor solubility, to **16d**, a potent CFTR activator with suitable solubility for eye drop formulation. Notably, **16d** was well distributed in target tissues including cornea and conjunctiva with minimal systemic exposure in rabbit. Topical ocular instillation of **16d** significantly enhanced tear secretion and improved corneal erosion in a mouse model of DED. In addition, **16d** significantly reduced mRNA expression of pro-inflammatory cytokines including IL-1 β , IL-17, and TNF- α and MMP2 in cornea and conjunctiva of DED mice.

INTRODUCTION

Dry eye disease (DED) is a multifactorial disease of the tears and ocular surface that results in symptoms of visual disturbance, discomfort, and tear-film instability with potential damage to the ocular surface.¹ The prevalence of DED has been reported to range from approximately 4.4 to 54.3%, making it one of the most prevalent diseases worldwide.^{2–5} Current advances in research on DED revealed that inflammatory processes are implicated in the pathogenesis of DED, suggesting a vicious cycle of ocular surface inflammation involving inflammatory cytokines and immune cells.^{6,7}

Considering the latest treatment for dry eye syndrome, artificial tears, which lubricate the ocular surface in a short time, are widely used preferentially, but there is a limitation in that it is a temporary relief effect rather than a fundamental treatment. To the next step, strategies targeting ocular surface inflammation, tear secretion, and meibomian gland dysfunction have been studied.⁸ However, so far, only two kinds of drugs, cyclosporine and lifitegrast (Figure 1), which inhibit T cell activation and

cytokine production, were approved as therapies for dry eye by U.S. Food and Drug Administration.^{9,10} Recently, diquafosol (Figure 1), P2Y₂ receptor agonist, is in the limelight as a next-generation treatment for DED. Diquafosol stabilizes the tear film by stimulating both fluid secretion from the conjunctival epithelial cells and mucin secretion from the goblet cells. In conjunctival epithelium, diquafosol stimulates fluid secretion through activation of calcium-activated chloride channels (CaCCs).^{11,12} Epithelial sodium channel (ENaC) inhibitor, P321, also came into spotlight as the next breakthrough of DED treatment by preserving lacrimal secretion and maintaining hydration in the ocular surface.¹³ Like these candidates, ion

Received: August 22, 2022

Published: December 27, 2022



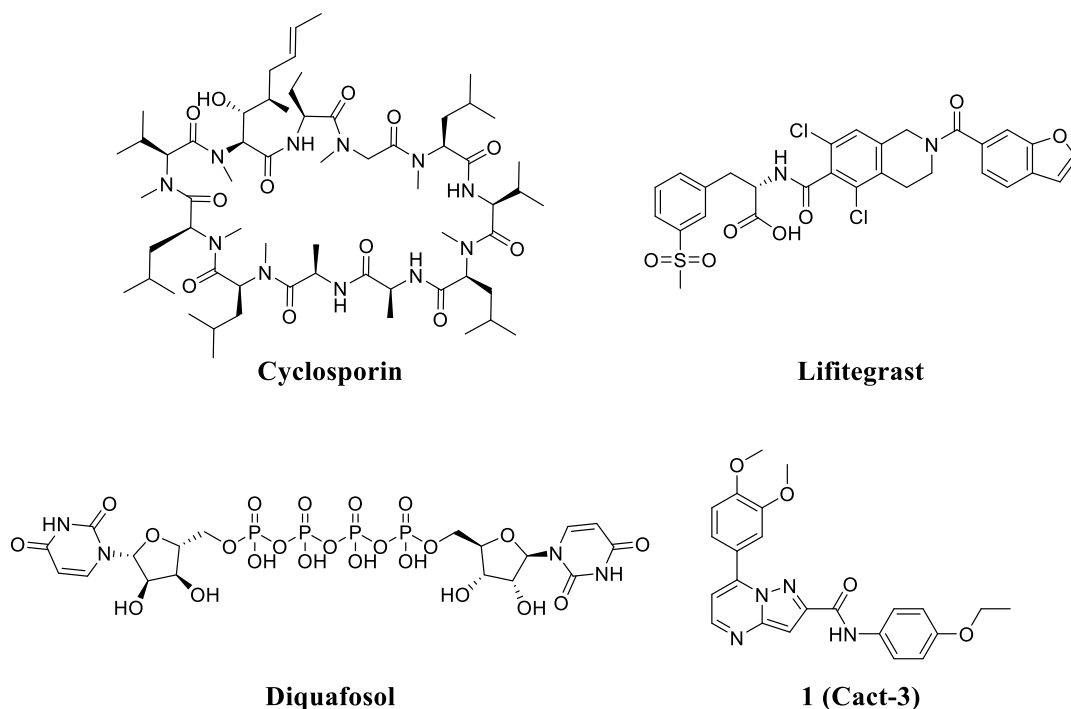


Figure 1. Structures of approved DED drugs and Cact-3.

channels expressed in the ocular epithelium and involved in the secretion of fluid and mucin are emerging as new targets for the development of DED therapeutics.^{14–16} From this perspective, we focused on the cystic fibrosis transmembrane conductance regulator (CFTR) chloride channel as a new therapeutic target for the treatment of DED. In our previous study, we identified a novel CFTR activator, Cact-3, that has good potency ($EC_{50} = 36.2$ nM) and selectivity.²² However, due to its poor solubility, Cact-3 needs to be optimized for development as an eye drop for the treatment of DED.

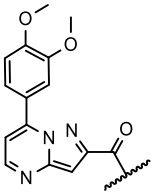
CFTR is activated *via* the cAMP signaling pathway and is expressed in a variety of secretory epithelia, including conjunctival and corneal epithelia, and activation of CFTR induces fluid secretion in mouse and human ocular surfaces.^{15,17,18} Cystic fibrosis (CF) patients, diagnosed by loss of functional mutation in CFTR, showed low tear film stability and ocular surface activity.^{19–21} In the human ocular surface, by measuring electric potential difference, robust CFTR activity was demonstrated.¹⁶ These results suggest the possibility that CFTR activators are potential candidates as the first-in-class agents for the treatment of DED.

Our previous study revealed that Cact-3 (**1**), a novel pyrazolo[1,5-*a*]pyrimidine analogue, is a promising activator of CFTR.²² Although Cact-3 showed nanomolar EC_{50} for CFTR activation (18 nM), it was sparingly soluble in phosphate-buffered saline (PBS) (59 nM) (Table 1). In ophthalmic drug discovery, aqueous solubility is one of the major factors influencing ocular bioavailability and ophthalmic formulation.²³ According to the rule of thumb for ophthalmic drugs (ROx) developed by Gukasyan *et al.*, the optimal calculated solubility for an effective ophthalmic drug should be 1 μ M or greater.²⁴ Since the nanomolar solubility of Cact-3 is a major hurdle for ophthalmic drug discovery, our synthetic strategy to develop an ophthalmic CFTR activator is to improve solubility while maintaining efficacy for CFTR. Herein, we report the synthesis

of **16d** and evaluation of its biological efficacy, plasma pharmacokinetics, ocular tissue distribution, and toxicity.

RESULTS AND DISCUSSION

General Synthetic Schemes for Pyrazolo[1,5-*a*]pyrimidine Analogues. The synthetic schemes for pyrazolo[1,5-*a*]pyrimidine analogs are depicted in Schemes 1–4. The enamine compound **2** was synthesized by the reaction of 3,4-dimethoxyacetophenone with DMF-DMA under reflux conditions. The carboxylic acid compound **4** was synthesized by cyclization of compound **2** with methyl 5-amino-1*H*-pyrazole-3-carboxylate to afford pyrazolo[1,5-*a*]pyrimidine ring, followed by hydrolysis. Using 3-[bis(dimethylamino)methyl]-3*H*-benzotriazol-1-oxide hexafluorophosphate (HBTU) as the coupling reagent, compounds **1** (Cact-3), **5a–h**, **12a–d**, and **14 a–l** were synthesized through the amide coupling between compound **4** and corresponding anilines or benzyl amines or amines. Compounds **5i–k** were synthesized *via* amide coupling between acid chloride intermediate and corresponding anilines. Compound **6** was synthesized *via* *tert*-butyldimethylsilyl (TBDMS) protection of methyl 4-amino-3-hydroxybenzoate. Compound **8** was synthesized *via* amide coupling between acid chloride intermediate and **6** to afford compound **7**, followed by TBDMS deprotection by tetra-*n*-butylammonium fluoride (TBAF). Hydrolysis of corresponding methyl esters afforded compounds **9a–b** and **13a–c**. Using HBTU as the coupling reagent, compounds **10a–d** were synthesized *via* amide coupling between compound **9a** and corresponding amines. Trifluoroacetic acid (TFA) or hydrogen chloride removal of Boc protecting group from compounds **10b–c** and **14d–g** afforded compounds **11a–b** and **15a–d**. HCl salt compound **11c** was synthesized from **10d** using hydrogen chloride. Compound **16a** was synthesized by the reaction of compound **15a** and benzyl bromide with potassium carbonate. Finally, compounds **16b–e** were synthesized *via* amide coupling between compounds **15a–d** and benzoyl chloride with pyridine.

Table 1. Activation of CFTR by Phenyl Analogues and Thermodynamic Solubility in PBS


Cpd	R	EC ₅₀ (nM) ^a	Solubility (nM) ^b	Solubility / YFP ratio	cLogD _{7.4} ^c
1 (Cact-3)		18	59	3	2.61
5a		65	ND ^d	-	2.75
5b		820	ND ^d	-	3.06
5c		31	ND ^d	-	2.72
5d		14	ND ^d	-	2.75
5e		6	ND ^d	-	2.17
5f		7	ND ^d	-	2.05
5g		470	ND ^d	-	2.72
5h		710	ND ^d	-	1.95
5i		17	ND ^d	-	2.84
5j		2,700	NT ^e	-	3.33
5k		>30,000	NT ^e	-	2.83
8		>30,000	NT ^e	-	1.91
9a		310	5,210	17	-0.09
9b		42	341	8	-0.30
10a		30	ND ^d	-	1.46
10b		17	ND ^d	-	2.43
10c		38	ND ^d	-	2.56
11a		3,700	NT ^e	-	0.70
11b		16,000	NT ^e	-	-0.42
11c		290	237,000	817	1.37

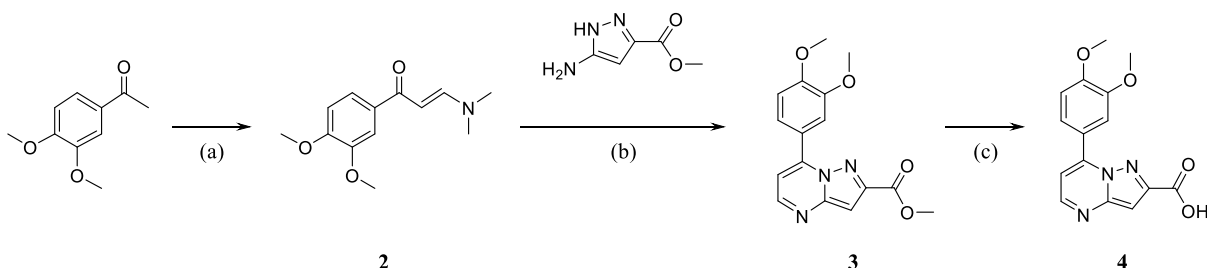
Table 1. continued

^aCFTR channel activity was measured by YFP quenching assay in CHO-K1 cells expressing human wild-type CFTR. The results are expressed as the mean of triplicates. ^bConcentration of the compound after 90 min of vortexing in PBS. ^ccLogD_{7.4} values were calculated by ACD/Percepta software (ACD/Labs, Toronto, Canada). ^dND: not detected. ^eNT: not tested.

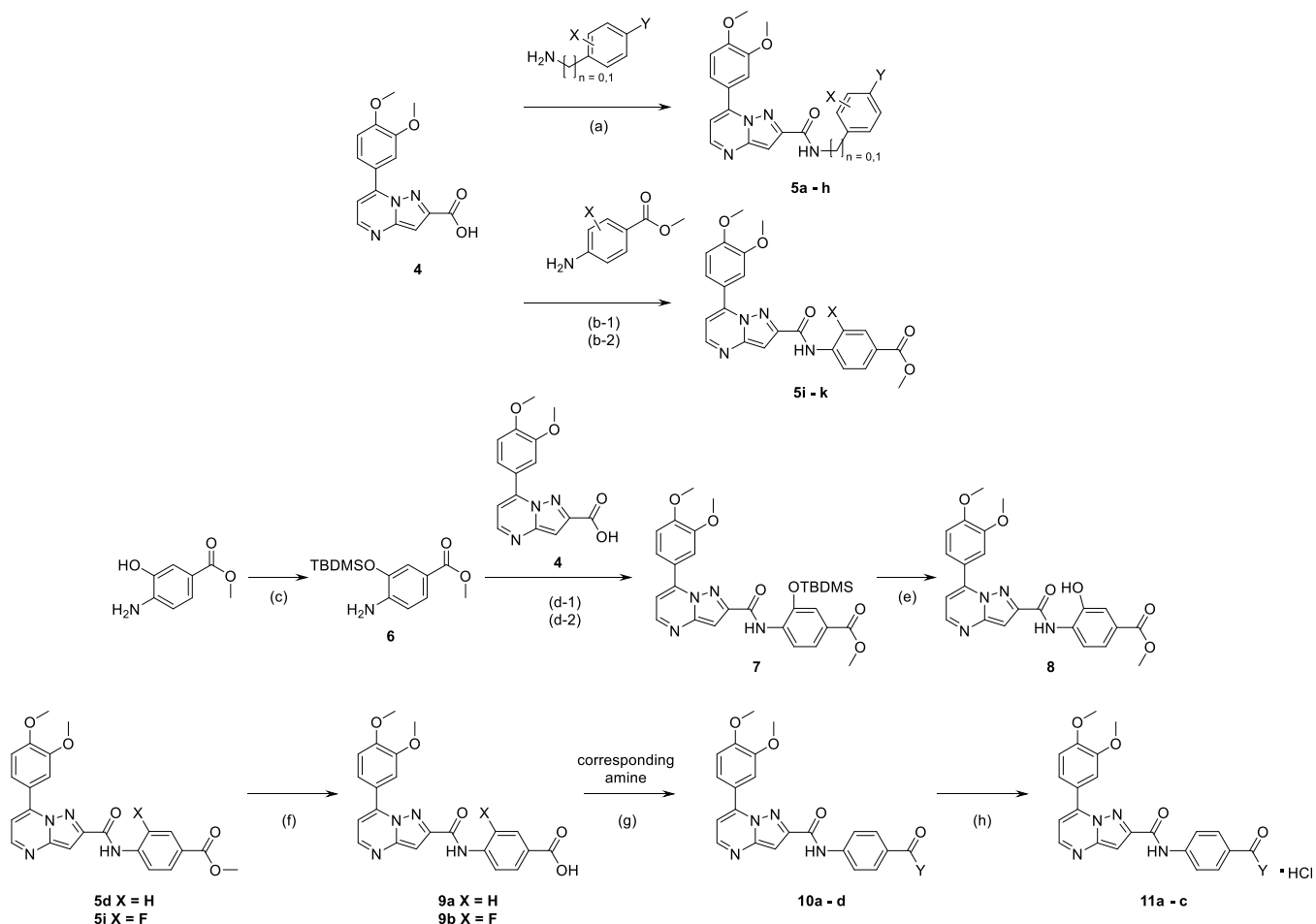
Molecular Docking Simulation and Preliminary Structure–Activity Relationship Analysis. Prior to structural optimization, we conducted a molecular docking simulation of Cact-3 with CFTR (PDB ID: 6O2P)²⁵ to establish synthetic strategy (Figure 2). According to docking simulation, hydrophobic interactions were formed between 3,4-dimethoxy moiety and Phe229, Phe316, and Leu233. In addition to hydrophobic interactions, the hydrogen bond was formed between the amide oxygen and Phe931. Molecular docking simulation has also revealed that 4-ethoxy phenyl moiety was exposed to the hydrophobic tail region of the lipid bilayer. We hypothesized that the highly hydrophilic moiety could cause repulsive interactions against the hydrophobic tail region and lead to decreased potency. In this study, we used cLogD_{7.4} as a descriptor of hydrophilicity.

Next, we prepared several pyrazolo[1,5-*a*]pyrimidine analogues to investigate essential moieties for potency. Summarized results are depicted in Figure 3 and Table S1. Preliminary structure–activity relationship (SAR) analysis was consistent with molecular docking simulation. 4-Methoxy moiety showed better efficacy than 3-methoxy moiety, and 3,4-dimethoxy was the best for biological efficacy. Replacing amide linker to inverted amide or urea led to decreased potency. Molecular docking simulation and preliminary SAR strongly suggests that 4-ethoxyphenyl is a suitable region for structural modification and cLogD_{7.4} is a key descriptor for potency. Therefore, our synthetic strategy is to find an appropriate LogD range that can retain potency and increase solubility at the same time.

Structure–Activity/Property Relationship Analysis of Cact-3 Analogues. Our first strategy to improve solubility was to introduce solubilizing group at the terminal phenyl ring. To investigate the optimal position on the phenyl ring, we introduced methyl ester moiety at ortho-(5b), meta-(5c), and para-(5d) positions. As shown in Table 1, 5d was more potent than 5b and 5c, with EC₅₀ values of 14, 820, and 31 nM, respectively. Notably, relatively bulky substituents, such as methyl ester, at the ortho-position could disrupt the active conformation and result in loss of potency. Further, we introduced a hydrophilic group at the para-position. Among them, 9a was 88-fold more soluble than Cact-3 (solubility values of 5210 and 59 nM, respectively) and 17-fold less potent than Cact-3 (EC₅₀ values of 310 and 18 nM, respectively). 5d and 9a results indicated that carboxylic acid moiety was too hydrophilic to retain potency. Therefore, we synthesized less hydrophilic compounds containing morpholine, piperazine, and amine. Morpholine-containing compounds (5e, 5f, and 10a) showed comparable potency over Cact-3 with EC₅₀ values of 6, 7, 30, and 18 nM, respectively, but they were completely insoluble (Table 1). Although 2-morpholinoethoxy group was known as a very soluble moiety, 5e was insoluble too. Because Cact-3 and its close analogues had a fully conjugated structure, solely introducing the solubilizing group at the terminal phenyl moiety was insufficient. Compounds 10b and 10c showed comparable potency to 10a because their hydrophilic amine moiety was

Scheme 1. Preparation of Compound 4^a

^aReagents and conditions: (a) DMF-DMA, DMF, reflux, 18 h; (b) AcOH, reflux, 2 h; (c) 1 N NaOH, H₂O, THF, MeOH, 60 °C, 2 h.

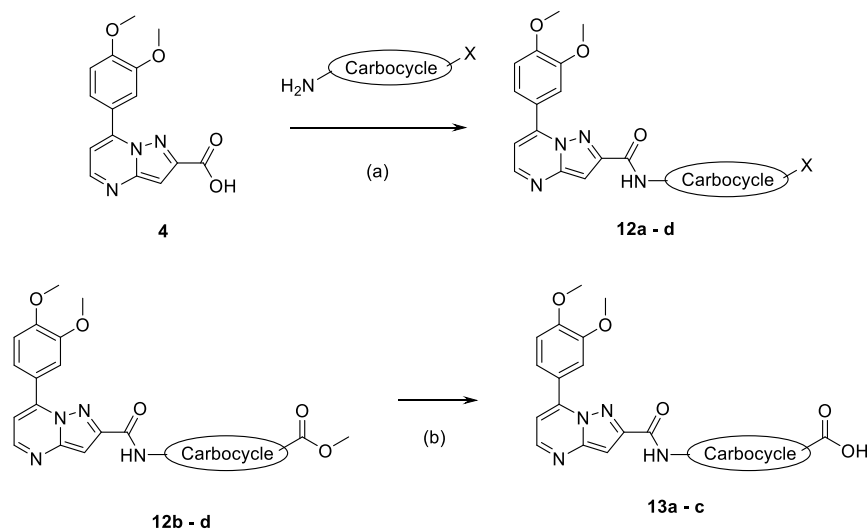
Scheme 2. Preparation of Compounds 5a–k, 8, 9a–b, 10a–d, and 11a–c^a

^aReagents and conditions: (a) HBTU, DIPEA, DCM, r.t., 24 h; (b-1) SOCl₂ (1 M in DCM), DCM, DMF, 60 °C, 2 h; (b-2) pyridine, DCM, 0 °C, 1 h; (c) TBDMSO, imidazole, 2.5 h; (d-1) SOCl₂ (1 M in DCM), DCM, DMF, 60 °C, 2 h; (d-2) pyridine, DCM, 0 °C, 1 h; (e) TBAF (1 M in THF), 0 °C, 1 h; (f) 1 N NaOH, THF, MeOH, H₂O, 60 °C, 2 h; (g) HBTU, DIPEA, DCM, r.t., 24 h; (h) HCl (4 N in dioxane), MeOH, r.t., 26 h.

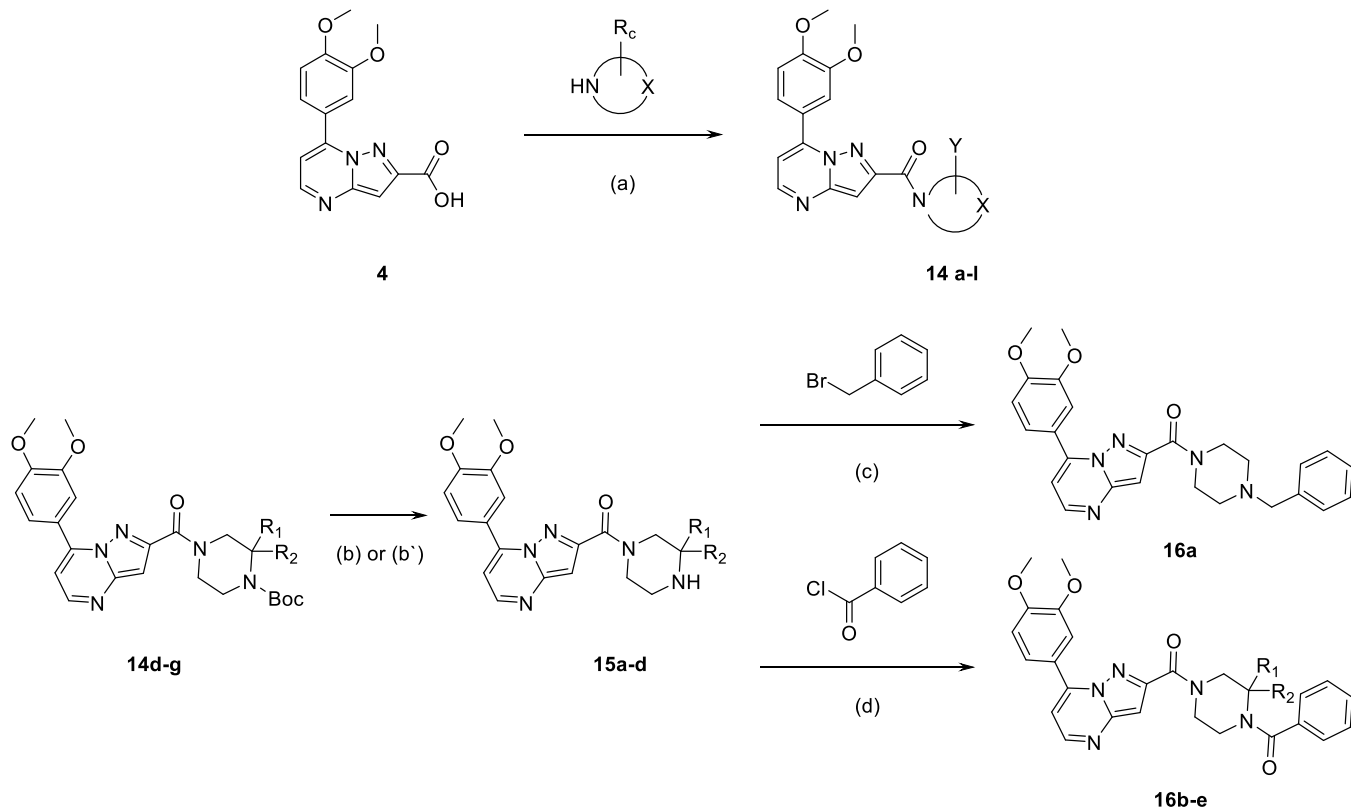
protected by the Boc group. However, deprotected compounds **11a** and **11b** had greatly reduced potency with EC₅₀ values of 3700 and 16,000 nM, respectively. We speculated that hydrophilic free amine moiety causes repulsive interactions between the compound and the hydrophobic tail of the membrane. To confirm the effect of hydrophilicity on potency, we introduced methyl moiety to the amine. Surprisingly, **11c** was 13-fold more potent than **11a**, with an EC₅₀ value of 290 nM. In addition, the solubility of **11c** was extremely increased with a solubility value of 237,000 nM. Although **11c** was 4017-fold more soluble than Cact-3, it was 16-fold less potent than

Cact-3. Therefore, the Sol/YFP ratio did not increase as much as the increased solubility.

The second strategy was the disruption of molecular planarity through an increased dihedral angle. We introduced functional groups at the ortho-position. As shown in Table 1, the introduction of an electron-donating group (**5k** and **8**) and a relatively large electron-withdrawing group (**5j**) led to decreased potency, whereas the introduction of the fluoro group (**5i**) retained potency, with an EC₅₀ value of 17 nM. We then prepared **9b** which had both fluoro and carboxylic acid groups. Remarkably, **9b** was 7 times more potent than **9a**, with EC₅₀ values for **9b** and **9a** of 42 and 310 nM, respectively. However,

Scheme 3. Preparation of Compounds 12a–d and 13a–c^a

^aReagents and conditions: (a) HBTU, DIPEA, DCM, r.t., 24 h; (b) 1 N NaOH, THF, MeOH, H₂O, 60 °C, 2 h.

Scheme 4. Preparation of Compounds 14a–l, 15a, and 16a–e^a

^aReagents and conditions: (a) HBTU, DIPEA, DCM, r.t., 24 h; (b) HCl (4 N in dioxane), MeOH, r.t., 26 h; (b') TFA, DCM, r.t., 4 h; (c) K₂CO₃, DMF, r.t., 3 h; (d) TEA, DCM, r.t., 24 h.

the solubility of **9b** was 341 nM; hence, its solubility/YFP ratio was 2-fold less than **9a**, with ratios of 8 and 17, respectively. We speculated that due to the electrostatic interaction between fluorine and adjacent N–H, molecular planarity was increased, and interactions with CFTR also increased. As a result, the solubility of **9b** was decreased, and the potency was increased.²⁶ We also introduced a carbon chain between the amide linker and the phenyl ring to increase molecular flexibility. As shown in

Table 1, **5g** and **5h** were 34-fold and 101-fold less potent than **5d** and **5f**, with EC₅₀ values of 470, 710, 14, and 7 nM, respectively. These results showed that the introduction of the carbon chain was not tolerated.

The third strategy was the removal of aromaticity. Replacing aromatic rings with carbocycle could reduce molecular planarity and also disrupt crystal-stacking capability.²⁷ Therefore, we first prepared **12a** to investigate whether modification of phenyl ring

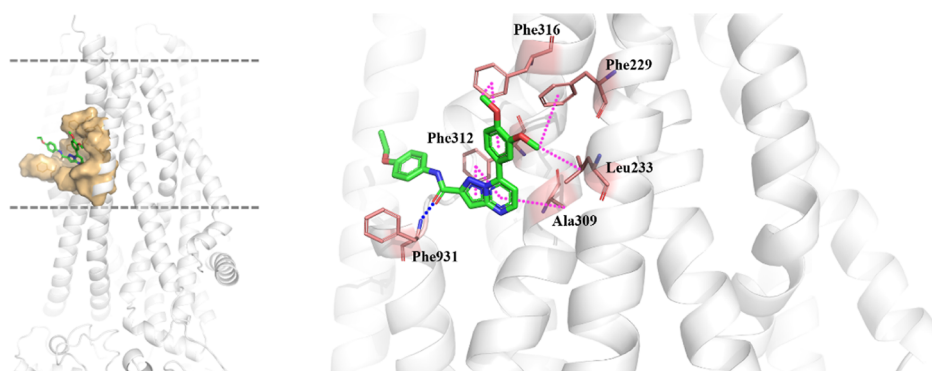


Figure 2. Molecular docking simulation of Cact-3 with CFTR (PDB ID: 6O2P). Blue dashed line indicates H-bond, and pink dashed line indicates hydrophobic interactions. Gray spiral ribbon indicates the hydrophobic tail region of the lipid bilayer.

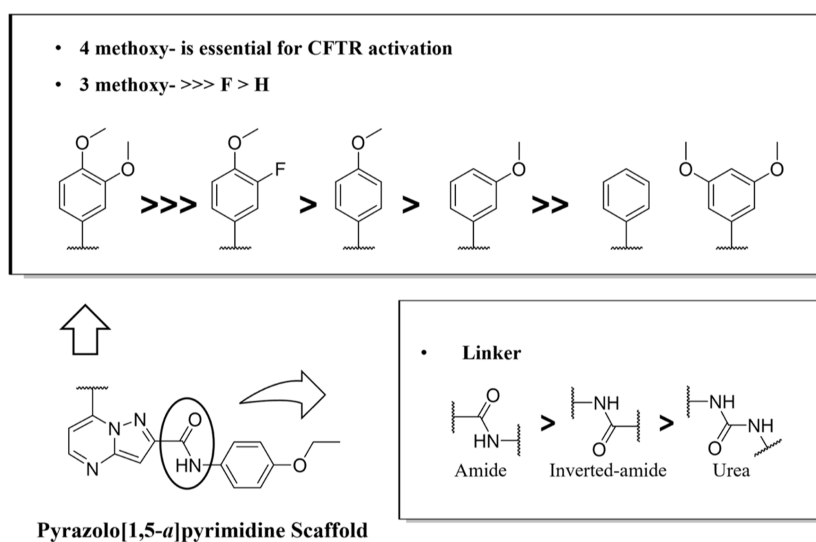
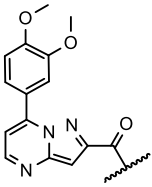


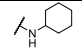
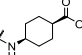
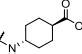
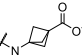
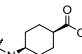
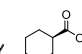
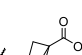
Figure 3. Preliminary SAR of pyrazolo[1,5-*a*]pyrimidine analogues.

to carbocycle was acceptable or not. As shown in Tables 1 and 2, **12a** had an EC_{50} value of 130 nM, which was comparable to that of **5a**. We further prepared *cis*-, *trans*-cyclohexyl analogues and bicyclo[1,1,1]pentane analogues. Interestingly, solubilities of **12b** and **12c** were improved when compared to **12a**, with solubility values of 7549, 1393 nM, and ND, respectively. These results suggested that introducing methyl ester moiety might disrupt crystal-staking capability, leading to increased solubility. We also prepared **13a**, **13b**, and **13c**. However, they completely lost potency. Again, we confirmed the effect of hydrophilicity on potency. Generally, introducing a hydrophilic group was a classical approach to improving solubility. However, as our target was membrane-embedded protein, we needed to figure out another approach rather than introducing hydrophilic moiety.

Replacing the terminal phenyl ring with carbocycle exerted a positive effect on solubility and a negative effect on potency at the same time. Based on these findings, we conducted further modifications to optimize potency. We introduced several heterocycles such as azetidine, pyrrolidine, piperidine, and piperazine. Table 3 shows that potency increased in the order of piperidine (**14c**) < azetidine (**14a**) < pyrrolidine (**14b**) < piperazine (**14d**), with EC_{50} values of 810, 700, 370, and 270 nM, respectively. To further investigate piperazine analogues, we replaced the Boc group with smaller moieties. De-Boc compound **15a** had greatly reduced potency with an EC_{50} value

of 17,000 nM. To adjust $cLogD_{7.4}$, we introduced hydrophobic moiety to the amine. Insertion of alkyl (**14i**, **14j**, **14k**) and cyclopropanecarbonyl (**14l**) moiety led to slightly increased potency. However, these compounds were still highly hydrophilic, so more hydrophobic moiety needed to be added. Therefore, we synthesized several phenyl analogues. **16b** with a carbonyl linker was 7-fold more potent than **16a**, with EC_{50} values of 110 and 730 nM. Besides, **16b** had a solubility/YFP ratio of 91, which is much higher than that of **9a**. We also conducted modifications to the piperazine ring. We added the *S*-methyl group (**16d**) to the piperazine ring, which led to a considerable increase in potency. Besides, **16d** (*S*-methyl) was 34-fold more potent than **16e** (*R*-methyl), with EC_{50} values of 23 and 790 nM, respectively. To explain potency difference, we conducted another molecular docking simulation (Figure 4). According to results, *S*-methyl moiety (**16d**) formed additional hydrophobic interactions with Phe316. Further, *R*-methyl moiety (**16e**) interfered with the hydrophobic interaction between the piperazine ring and Phe312. Therefore, **16d** could interact with CFTR more efficiently than **16e** with calculated binding energy values of -70.7 and -54.2 kcal/mol. Furthermore, **16d** was 13-fold more soluble than **16b**, with solubility values of 134, 489 and 10,053 nM. We speculated that *S*-methyl moiety would disrupt molecular planarity and symmetry and lead to extremely increased solubility.²⁷ Through the strategic optimization, we identified **16d** which had a

Table 2. Activation of CFTR by Carbocycle Analogues and Thermodynamic Solubility in PBS


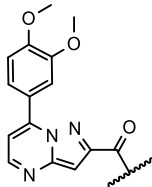
Cpd	R	EC ₅₀ (nM) ^a	Solubility (nM) ^b	Solubility / YFP ratio	cLogD _{7,4} ^c
12a		130	ND ^d	-	2.47
12b		590	7,549	13	1.97
12c		180	1,393	8	1.97
12d		310	1,418	5	1.33
13a		>30,000	NT ^e	-	-1.04
13b		>30,000	NT ^e	-	-1.04
13c		>30,000	NT ^e	-	-2.18

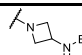
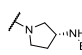
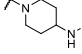
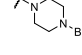
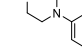
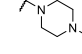
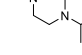
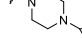
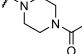
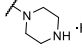
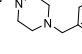
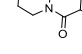
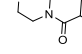
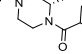
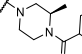
^aCFTR channel activity was measured by YFP quenching assay in CHO-K1 cells expressing human wild-type CFTR. The results are expressed as the mean of triplicates. ^bConcentration of the compound after 90 min of vortexing in PBS. ^ccLogD_{7,4} values were calculated by ACD/Percepta software (ACD/Labs, Toronto, Canada). ^dND: not detected. ^eNT: not tested.

comparable *in vitro* efficacy over Cact-3 and had a sub-millimolar solubility (Figure 5). Thus, we chose **16d** as the best compound for pharmacological and functional studies.

Effect of 16d on CFTR Chloride Channel Activity. To investigate the effect of **16d** on CFTR chloride channel activity, apical membrane currents were measured in FRT cells expressing human CFTR. **16d** potentially activated CFTR chloride channel in a dose-dependent manner with an EC₅₀ of 342 nM, and the **16d**-induced CFTR chloride current was completely blocked by CFTR_{inh}-172, a potent and selective inhibitor of CFTR (Figure 6A,B). To further characterize the activation of CFTR by **16d**, whole-cell patch-clamp analysis was performed on CHO-K1 cells expressing human CFTR. Application of 30 μM **16d** strongly activated CFTR currents, exhibiting a linear current/voltage relationship like forskolin-induced activation of CFTR, and the **16d**-induced CFTR currents were completely inhibited by CFTR_{inh}-172 (Figure 6C–E).

In Vitro Characterization of 16d. To investigate the effect of **16d** on other chloride channels, we observed the effect of **16d** on calcium-activated chloride channel TMEM16A/Anoctamin 1 (ANO1) and volume-regulated anion channel (VRAC). ANO1 apical membrane currents were measured in FRT cells expressing human ANO1, and VRAC activity was measured

Table 3. Activation of CFTR by Heterocycle Analogues and Thermodynamic Solubility in PBS


Cpd	R	EC ₅₀ (nM) ^a	Solubility (nM) ^b	Solubility / YFP ratio	cLogD _{7,4} ^c
14a		700	NT ^e	-	1.66
14b		370	NT ^e	-	1.80
14c		810	NT ^e	-	2.13
14d		270	NT ^e	-	1.98
14h		840	ND ^d	-	2.32
14i		8,100	NT ^e	-	0.72
14j		6,000	NT ^e	-	1.16
14k		1,400	NT ^e	-	0.87
14l		1,700	NT ^e	-	0.86
15a		17,000	NT ^e	-	-0.14
16a		730	NT ^e	-	2.17
16b		110	10,053	91	1.46
16c		200	1,816	9	2.06
16d		23	134,489	5,847	1.73
16e		790	158,586	201	1.73

^aCFTR channel activity was measured by YFP quenching assay in CHO-K1 cells expressing human wild-type CFTR. The results are expressed as the mean of triplicates. ^bConcentration of the compound after 90 min of vortexing in PBS. ^ccLogD_{7,4} values were calculated by ACD/Percepta software (ACD/Labs, Toronto, Canada). ^dND: not detected. ^eNT: not tested.

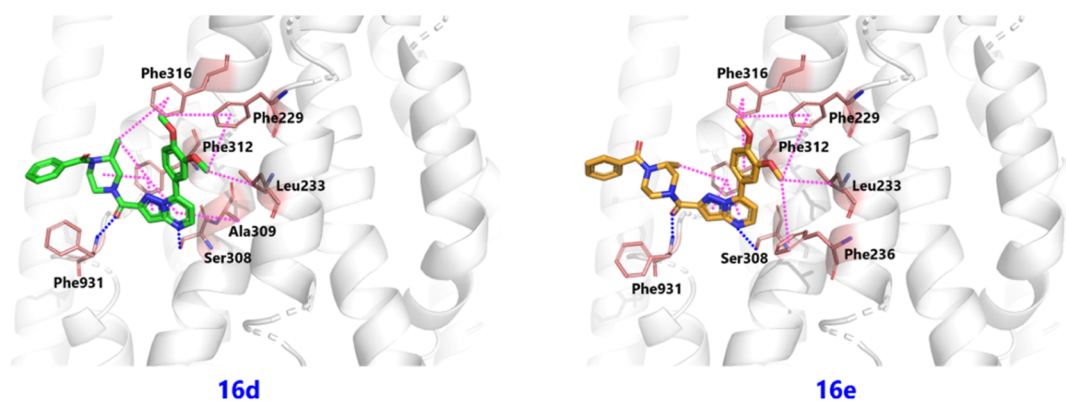


Figure 4. Molecular docking simulation of **16d** and **16e** with CFTR (PDB ID: 6O2P). Blue dotted line indicates H-bond, and pink dotted line indicates hydrophobic interactions. Gray spiral ribbon indicates the hydrophobic tail region of the lipid bilayer.

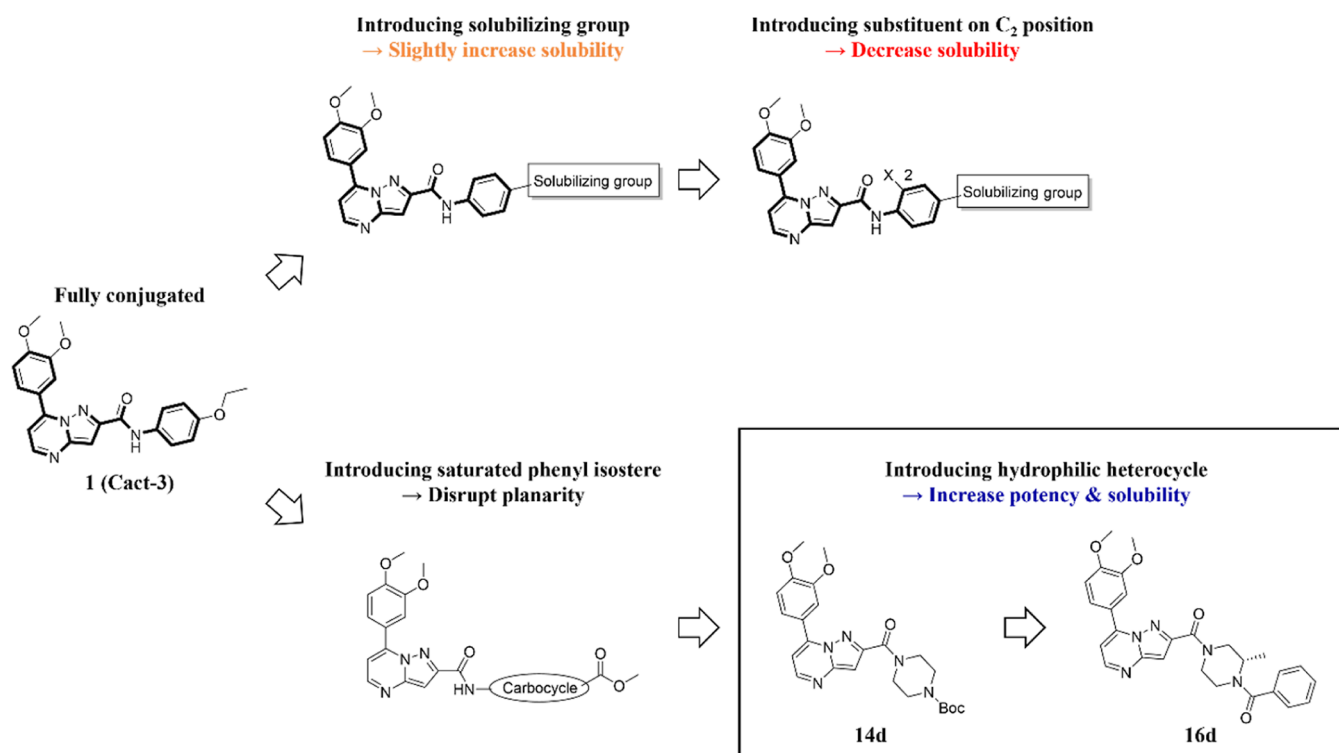


Figure 5. Strategic optimization scheme.

using YFP fluorescence quenching assay in LN215 cells expressing a halide sensors YFP-F46L/H148Q/I152L. A high concentration ($30\ \mu\text{M}$) of **16d** did not affect channel activities of ANO1 and VRAC, but ANO1 and VRAC were completely blocked by Ani9²⁸ and VI-116,²⁹ respectively (Figure 7A,B). CFTR is activated by cAMP signaling pathway. Therefore, we observed the effect of **16d** on intracellular cAMP concentration. **16d** slightly increased cAMP level compared to the control but did not increase cAMP level as strongly as forskolin (Figure 7). To observe the cytotoxicity of **16d**, the effect of **16d** on cell viability was evaluated in the corneal epithelial (CorE) and conjunctival epithelial (ConjE) cells. **16d** did not affect the cell viability of CorE and ConjE at $30\ \mu\text{M}$ (Figure 7D). To investigate whether **16d** could activate endogenous CFTR channels in human ocular epithelium, short-circuit current was measured in primary cultured human conjunctival epithelial cells. Interestingly, **16d** potently increased CFTR-dependent chloride current in a dose-dependent manner, and the **16d**-

induced CFTR current was fully inhibited by $10\ \mu\text{M}$ CFTR_{inh}-172. These results suggest that **16d** can potently and selectively activate human CFTR without cytotoxicity in ocular epithelium.

Ocular Distribution and Plasma Pharmacokinetics of 16d. Before investigating *in vivo* efficacy of **16d**, ocular tissue distribution and plasma pharmacokinetics (PK) after topical ocular administration of **16d** in male New Zealand White Rabbit were evaluated. No adverse effects of **16d** were observed during the PK study. As shown in Figure 8 and Table 4, the **16d** concentrations of tear, cornea, and conjunctiva were maintained above the EC₅₀ value of $342\ \text{nM}$ ($166\ \text{ng/mL}$) for 8 h. For mean plasma concentrations of **16d**, PK parameters were not determined because they were below the lower limit of quantitation up to 72 h except for 0.5 h following administration. These results indicate that **16d** is well distributed in CFTR-expressing target tissues (cornea and conjunctiva), is maintained for a long period of time, and has a negligible systemic exposure.

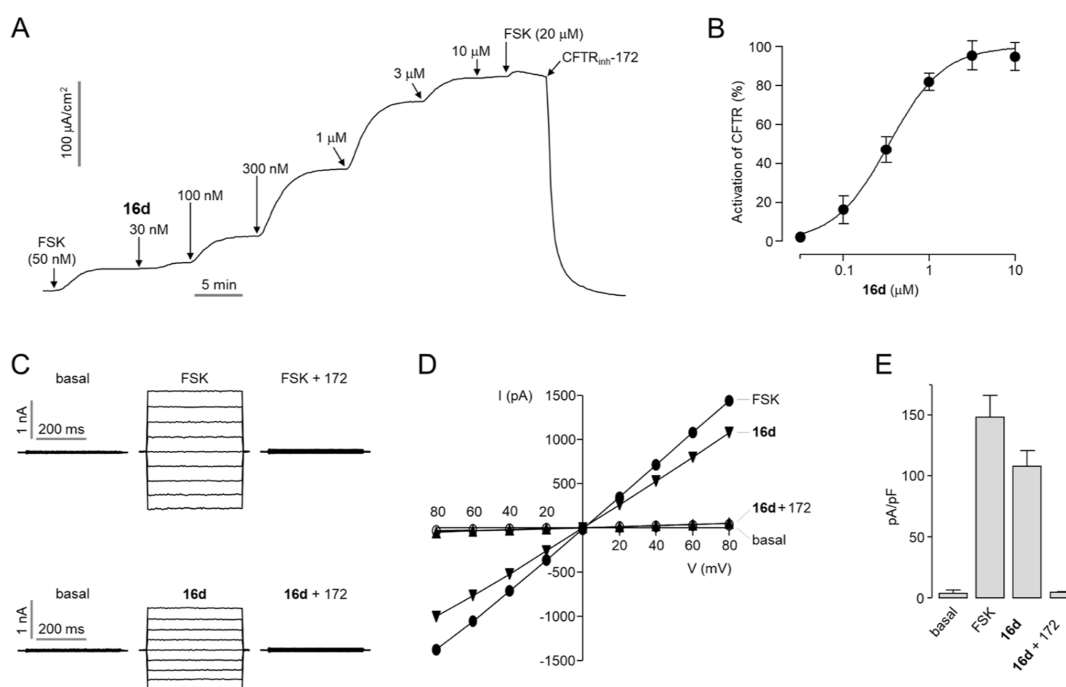


Figure 6. Activation of CFTR chloride channels by **16d**. (A) Representative trace of apical membrane current in FRT cells expressing human CFTR. CFTR was activated by the indicated concentrations of **16d** in the presence of 50 nM forskolin (FSK) and inhibited by 10 μM CFTR_{inh}-172. (B) Summary of CFTR activation (mean ± S.E., *n* = 3). (C) Whole-cell currents were recorded at a holding potential of 0 mV and pulsed with voltages between ±80 mV (in steps of 20 mV) in CHO-K1 cells expressing human CFTR. CFTR was activated by 20 μM forskolin or 30 μM **16d** and inhibited by 20 μM CFTR_{inh}-172. (D) Current/voltage plot of mean currents at the middle of each voltage pulse. (E) Summary of current density at +80 mV (mean ± S.E., *n* = 3).

16d Shows Faster Action and Higher Maximal Efficacy Compared to Cact-3. To investigate the pharmacological advantages of **16d** compared with Cact-3, we observed the effect of **16d** and Cact-3 on tear volume in normal female C57BL/6J mice. The maximum solubility of Cact-3 was 72 μM, so Cact-3 was administered up to 72 μM. In the case of **16d**, the maximum solubility was greater than 2 mM, and **16d** was administered up to 1 mM. As shown in Figure 9, treatment of both **16d** and Cact-3 showed a dose-dependent increase in tear volume, and E_{\max} of **16d** was higher than Cact-3; **16d** reached maximal tear volume at 1 h after administration, whereas Cact-3 showed maximal tear volume at 3 h after administration. Thus, **16d** has the advantage of higher solubility, higher maximal efficacy, and faster action compared to Cact-3.

Enhancing Tear Volume and Reduction of Corneal Erosion by 16d in DED Mice. To investigate the effect of **16d** on tear volume in DED mice, tear volume was evaluated by phenol red thread test in scopolamine-induced dry eye mouse model. As shown in Figure 10A, subcutaneous injection of scopolamine significantly reduced the thread wetting length in both no treatment and vehicle-treated groups compared to control group. However, treatment of **16d** significantly and almost completely restored the scopolamine-induced tear volume decrease, and diquafosol also showed a significant recovery in tear volume in DED mice. To investigate whether **16d** ameliorated ocular surface damage in DED mice, we observed changes in corneal erosion in scopolamine-induced dry eye mouse models treated with the vehicle, **16d**, or diquafosol. Each eye drop was applied to each eye three times a day for 10 days. **16d** significantly reduced corneal erosion compared to control group (Figure 10B,C). These results reveal that **16d**

enhances the tear secretion and reduces corneal erosion in DED mice with an efficacy equal to or greater than that of diquafosol.

Reduction of mRNA Expression of Pro-Inflammatory Cytokines and MMP2 by 16d in Ocular Epithelium of DED Mice. The ocular surface of DED is known to exhibit high levels of infectious cytokines such as IL-1β, IL-6, IL-17, and TNF-α as well as matrix-metalloproteinase (MMP)-2 and MMP-9. In cornea and conjunctiva of normal or DED mice, the mRNA expression levels of MMP-2, MMP-9 and pro-inflammatory cytokines including IL-1β, IL-6, IL-17, and TNF-α were investigated by real-time PCR in the presence or absence of the vehicle, **16d**, and diquafosol. The mRNA expression levels of IL-1β, IL-17, TNF-α, and MMP-2 in cornea and conjunctiva were significantly decreased when treated with **16d** (Figure 11). Among them, the mRNA expression levels of IL-17, TNF-α, and MMP-2 were also significantly reduced by diquafosol. These results reveal that **16d** reduces the mRNA expression levels of IL-1β, IL-17, TNF-α, and MMP-2 in cornea and conjunctiva of DED mice with an efficacy equal to or greater than that of diquafosol.

CONCLUSIONS

The goal of this study was to improve the poor solubility of Cact-3 for the development of new therapeutic agents for DED because it is important to have good solubility in order to achieve high ocular bioavailability and reduce ocular surface damage. To improve solubility of Cact-3, we conducted structural modification of Cact-3 (1). Synthetic strategies were as follows: (i) introducing hydrophilic moiety on phenyl ring, (ii) introducing carbon linker between amide and phenyl ring, (iii) introducing saturated phenyl isostere, and (iv) introducing the hydrophilic heterocycle. The first and second strategies were

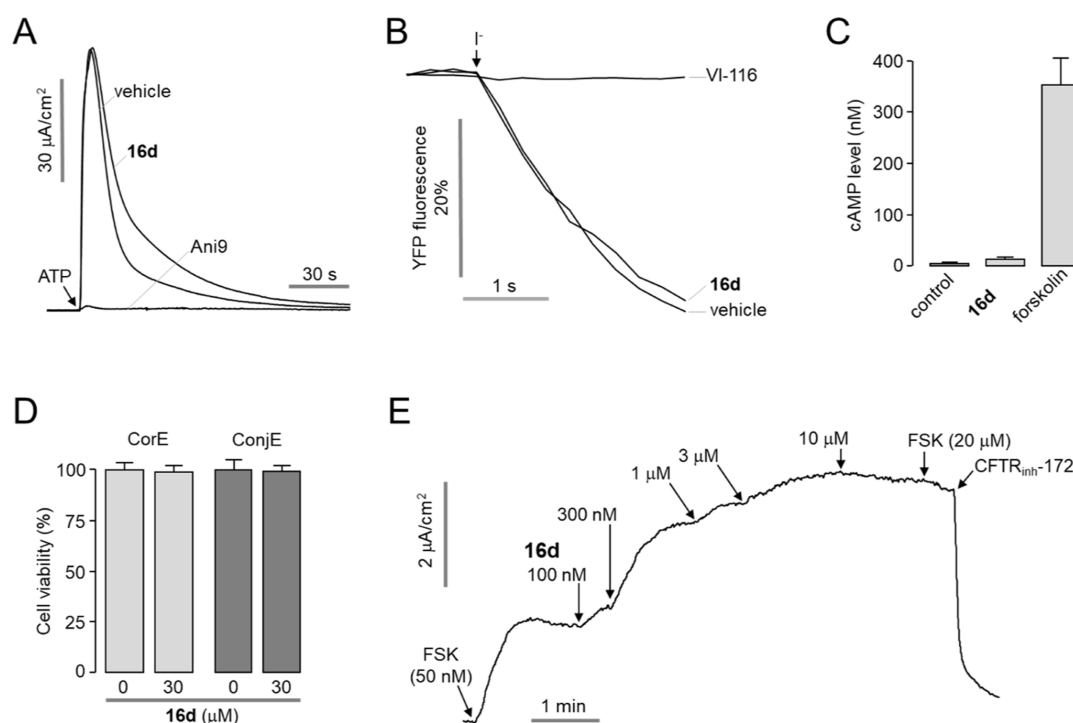


Figure 7. Characterization of **16d** and its effect on CFTR activity in primary cultured human conjunctival epithelial cells. (A) Apical membrane current was measured in ANO1 expressing FRT cells. ANO1 was activated by 100 μM ATP and inhibited by 10 μM Ani9, an ANO1 inhibitor. Cells were pretreated with **16d** (30 μM) and Ani9 for 10 min. (B) Effect of **16d** on VRAC chloride channel activity was observed in YFP-F46L/H148Q/I152L expressing HeLa cells. Cells were treated with **16d** (30 μM) in hypotonic solution for 5 min. VRAC was inhibited by 10 μM VI-116, a VRAC inhibitor. (C) CHO-K1 cells were treated with **16d** (30 μM) and forskolin (10 μM) in the presence of IBMX (100 μM) for 10 min, and then cAMP levels were determined (mean \pm S.E., $n = 3$). (D) Corneal epithelial (CorE) and conjunctival epithelial (ConjE) cells were treated with **16d** for 48 h, and cell viability was determined by MTS assay (mean \pm S.E., $n = 3$). (E) Representative trace of short-circuit current in primary cultured human conjunctival epithelial cells. CFTR was activated by the indicated concentrations of **16d** and blocked by 10 μM CFTR_{inh}-172.

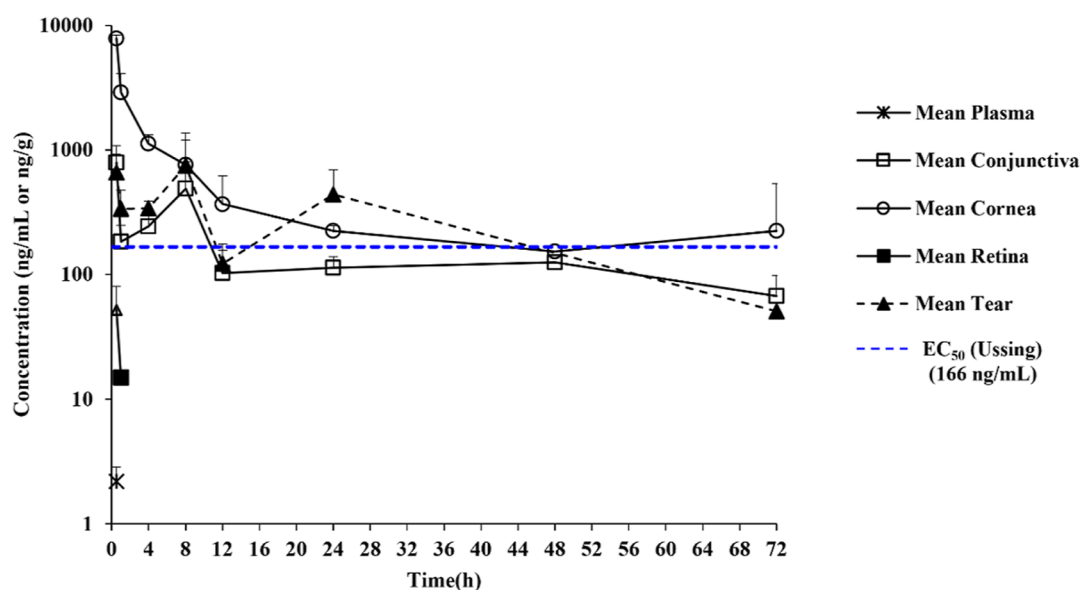


Figure 8. Mean concentration–time profiles of **16d** in rabbit after single topical instillation of **16d** eye drops at 0.1 mg/eye.

not effective to improving solubility. Through the third approach, we figured out the positive effect on potency and solubility. Finally, we introduced piperazine ring into the pyrazolo[1,5-*a*]pyrimidine scaffold, and further optimization of the piperazine ring identified a potent and highly soluble CFTR activator, **16d**, with desirable PK profiles.

Notably, electrophysiological studies demonstrated that **16d** potently and selectively activated CFTR chloride channel without cytotoxicity of corneal and conjunctival epithelial cells. In addition, **16d** was well distributed and maintained for a long period of time (>8 h) in cornea and conjunctiva of rabbit, and systemic exposure was negligible. In the following *in vivo* experiments, **16d** significantly enhanced tear volume restoration

Table 4. Mean Pharmacokinetic Parameters of 16d in Rabbit after Single Topical Instillation of 16d Eye Drops at 0.1 mg/Eye ($n = 3$)

PK parameters	mean plasma	mean conjunctiva	mean cornea	mean retina	mean tear
C_{\max} (ng/mL or ng/g)	ND ^a	793.0	7840.0	ND ^a	749.0
T_{\max} (h)	ND ^a	0.5	0.5	ND ^a	8.0
$T_{1/2}$ (h)	ND ^a	40.6 ^b	23.1 ^b	ND ^a	29.8 ^b
T_{last} (h)	ND ^a	72.0	72.0	ND ^a	72.0
AUC _{0-last} (ng·h/mL or ng·h/g)	ND ^a	9819.0	28349.0	ND ^a	16573.0
AUC ₀₋₂₄ (ng·h/mL or ng·h/g)	ND ^a	4734.0	19409.0	ND ^a	7952.0
AUC _{0-inf} (ng·h/mL or ng·h/g)	ND ^a	13741.0	35802.0	ND ^a	18750.0

^aND: not determined (parameters not determined due to an inadequately defined terminal elimination phase). ^bThe adjusted linear regression coefficient of the concentration value on the terminal phase is less than 0.9; $T_{1/2}$ might not be accurately estimated. Composite mean concentration was used in PK parameter calculation.

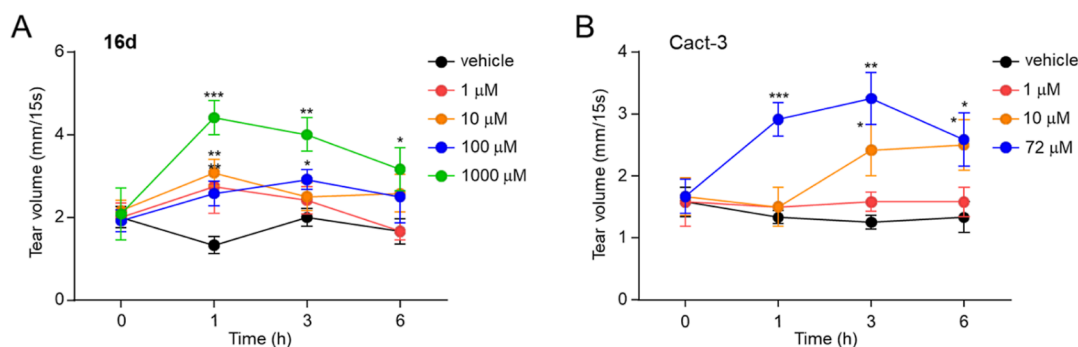


Figure 9. Effect of 16d and Cact-3 on tear volume in normal mice. (A) Tear volume was measured in each group treated with 16d at different concentrations by phenol red thread test (mean \pm S.E., $n = 6$). (B) Tear volume was measured in each group treated with Cact-3 at different concentrations by phenol red thread test (mean \pm S.E., $n = 6$). Mice were treated with 2.5 μ L eye drops of the vehicle (5% polyoxyl 35 castor oil in sodium phosphate buffer), 16d, and Cact-3. * $p < 0.05$, ** $p < 0.01$, *** $p < 0.001$.

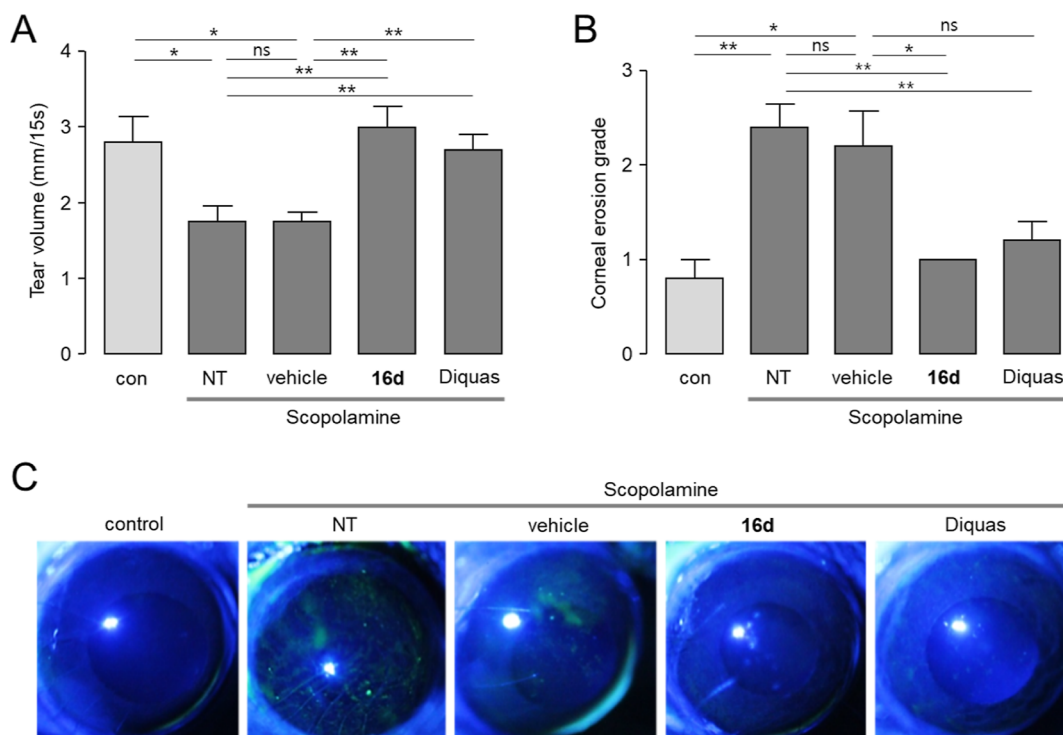


Figure 10. Effect of 16d on tear volume and ocular surface damage in scopolamine-induced dry eye mouse model. (A) Tear volume of each group was measured with phenol red thread test (mean \pm S.E., $n = 5$). (B) Corneal erosion grade of each group was measured by fluorescein staining on a five-point scale (mean \pm S.E., $n = 5$). (C) Representative images of corneal fluorescein-stained mouse eyes. Mice were treated with 5 μ L of eye drops of the vehicle (5% polyoxyl 35 castor oil in sodium phosphate buffer), 16d (2060 μ M), and diquafosol three times a day for 10 days while maintaining the dry eye condition. NT: no treatment; Diquas: diquafosol; ns: not significant. * $p < 0.05$, ** $p < 0.01$.

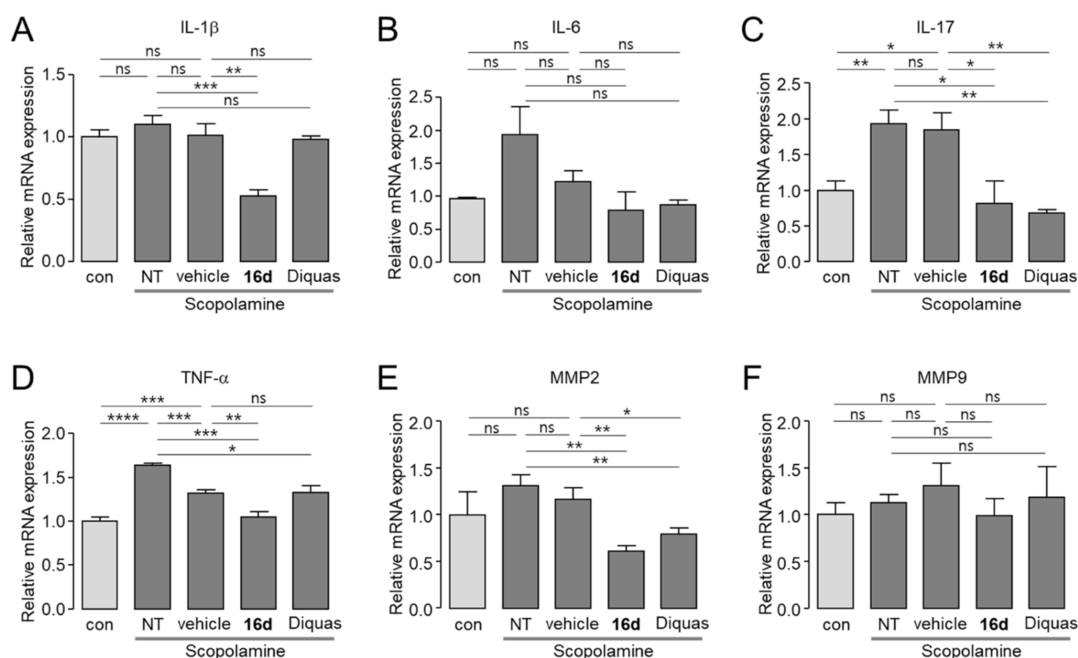


Figure 11. Effect of **16d** on the mRNA expression levels of pro-inflammatory cytokines and MMPs in cornea and conjunctiva. (A–F) mRNA expression level of IL-1 β , IL-6, IL-17, TNF- α , MMP2, and MMP9 in cornea and conjunctiva. Mice were treated with 5 μ L of eye drops of the vehicle (5% polyoxyl 35 castor oil in sodium phosphate buffer), **16d** (2060 μ M), and diquafosol three times a day for 10 days while maintaining the dry eye condition (mean \pm S.E., $n = 5$). NT: no treatment; diquas: diquafosol; ns: not significant. * $p < 0.05$, ** $p < 0.01$, *** $p < 0.001$, **** $p < 0.0001$.

and improved corneal erosion in scopolamine-induced dry eye mice comparable to diquafosol. **16d** also significantly reduced mRNA expression levels of MMP2 and pro-inflammatory cytokines including IL-1 β , IL-17, and TNF- α in cornea and conjunctiva of scopolamine-induced dry eye mice. Taken together, these results suggest that **16d** will shed light on the development of novel therapeutic agent for DED.

EXPERIMENTAL SECTION

All commercially available solvents and reagents were used without further purification. Reactions were monitored by thin-layer chromatography (TLC) using precoated TLC Silica gel (Merck, 60 F₂₅₄). Column chromatography was carried out by MPLC (Combi-Flash) using prepacked silica gel columns (Agela technologies, 40–60 μ M, spherical particles). UPLC/MS was carried out using a Waters Acquity UPLC system with an Acquity PDA detector (UV = 210–400 nm) and Acquity QDa detector. The flow rate was 0.2 mL/min, and the solvent system was [95% A + 5% B] to [5% A + 95% B] (A = 0.1% formic acid in water, B = 0.1% formic acid in MeOH). An Acquity UPLC BEH C18 column (1.7 μ m, 2.1 \times 50 mm column) was used. ¹H and ¹³C NMR spectra were recorded on a Bruker ascend 400 spectrometer (400 MHz for ¹H NMR and 100 MHz for ¹³C NMR). All spectra were recorded in commercially available deuterated solvents (CDCl₃, DMSO-*d*₆, Cambridge isotope laboratories). Chemical shifts (δ) for ¹H and ¹³C NMR are in parts per million. Abbreviations representing multiplicity are reported as follows: s = singlet, d = doublet, t = triplet, q = quartet, and m = multiplet. HRMS was carried out using a JMS-T200GC with a field desorption probe (mass range $m/z \sim 1000$). HPLC was done on a YMC-Pack ODS-A column (4.6 mm \times 150 mm, 5 μ m) with 1.0 mL/min water/acetonitrile (containing 0.05% trifluoroacetic acid), 40 min linear gradient, 20–100% acetonitrile. UV absorbance was detected at 290 nm. The purity of final compounds was determined to be above 95% by this method, with exception of compounds **5b** (not detectable), **5h** (93%), **5i** (85%), **5j** (not detectable), **8** (not detectable), **9a** (not detectable), **9b** (not detectable), **11c** (92%), **14b** (not detectable), and **14h** (not detectable). However, their purity and structure were analyzed by NMR, UPLC-MS, and HRMS. The results are consistent with

structures. Melting points were determined on an MPA100 Optimelt automated melting point system by Stanford Research Systems without correction, and the values were written as a single point.

Compounds for preliminary SAR are described in the [Supporting Information](#).

(E)-1-(3,4-Dimethoxyphenyl)-3-(dimethylamino)prop-2-en-1-one (2). 3',4'-Dimethoxyacetophenone (0.29 mL, 2.5 mmol) and DMF-DMA (1.33 mL, 10 mmol) were combined in DMF (2.50 mL) and heated to reflux for 18 h. The reaction mixture was extracted by DCM and aq NH₄Cl. The organic layer was dried over anhydrous MgSO₄ and concentrated. The mixture was extracted by EA and aq NH₄Cl to give **2** (193 mg, 43%) as a yellow solid. ¹H NMR (400 MHz, DMSO-*d*₆) δ 7.67 (d, $J = 12.0$ Hz, 1H), 7.54 (dd, $J = 8.4, 2.0$ Hz, 1H), 7.45 (d, $J = 2.0$ Hz, 1H), 6.97 (d, $J = 8.4$ Hz, 1H), 5.83 (d, $J = 12.0$ Hz, 1H), 3.81 (s, 3H), 3.81 (s, 3H), 3.13 (s, 3H), 2.91 (s, 3H); MS-ESI m/z 237 [MH⁺].

Methyl 7-(3,4-dimethoxyphenyl)pyrazolo[1,5-a]pyrimidine-2-carboxylate (3). **2** (190 mg, 1.08 mmol) and methyl 5-amino-1H-pyrazole-3-carboxylate (152 mg, 1.08 mmol) were dissolved in acetic acid (5.40 mL) and heated to reflux for 2 h. The reaction mixture was extracted by DCM and aq NaHCO₃. The organic layer was dried over anhydrous MgSO₄ and concentrated. The reaction mixture was purified by MPLC, elution gradient 0 to 50% EA in hexane. The crude mixture was solidified by using DCM and hexane to give **3** (87.8 mg, 32%) as a white solid. ¹H NMR (400 MHz, DMSO-*d*₆) δ 8.69 (d, $J = 4.4$ Hz, 1H), 7.87 (dd, $J = 8.6, 2.4$ Hz, 1H), 7.78 (d, $J = 2.4$ Hz, 1H), 7.46 (d, $J = 4.4$ Hz, 1H), 7.25 (s, 1H), 7.21 (d, $J = 8.8$ Hz, 1H), 3.91 (s, 3H), 3.89 (s, 3H), 3.87 (s, 3H); MS-ESI m/z 314 [MH⁺].

7-(3,4-dimethoxyphenyl)pyrazolo[1,5-a]pyrimidine-2-carboxylic Acid (4). **3** (915 mg, 2.92 mmol) was dissolved in H₂O/THF/MeOH (12/20/10 mL), followed by addition of sodium hydroxide in H₂O (1 N, 5.84 mL) and stirring at 60 $^{\circ}$ C for 2 h. After cooling at 0 $^{\circ}$ C, the mixture was acidified by adding 1 N HCl. Then the precipitated crystals were filtered out by using H₂O to give **4** (980 mg, >99%) as a pale-yellow solid. ¹H NMR (400 MHz, DMSO-*d*₆) δ 13.35 (s, 1H), 8.68 (d, $J = 4.4$ Hz, 1H), 7.90 (dd, $J = 8.4$ Hz, 2.0 Hz, 1H), 7.80 (d, $J = 2.0$ Hz, 1H), 7.44 (d, $J = 4.4$ Hz, 1H), 7.22–7.20 (m, 2H), 3.89 (s, 3H), 3.87 (s, 3H); MS-ESI m/z 300 [MH⁺].

7-(3,4-Dimethoxyphenyl)-N-(4-ethoxyphenyl)pyrazolo[1,5-a]pyrimidine-2-carboxamide. (**1**, Cact-3) **4** (6000 mg, 20.04

mmol), *p*-phenetidine (2.84 mL, 22.04 mmol), HBTU (8359 mg, 22.04 mmol), and diisopropylethylamine (6.91 mL, 40.08 mmol) were combined in DCM (200 mL). After stirring for 24 h at r.t., the reaction mixture was extracted by DCM and aq NaHCO₃. The reaction mixture was purified by MPLC, elution gradient 20 to 50% EA in hexane. The crude mixture was solidified using EA and hexane to give **1** (4360 mg, 51%) as a white solid. ¹H NMR (400 MHz, CDCl₃) δ 8.76 (s, 1H), 8.58 (d, *J* = 4.3 Hz, 1H), 7.70–7.65 (m, 2H), 7.62–7.57 (m, 2H), 7.40 (s, 1H), 7.10 (d, *J* = 8.2 Hz, 1H), 7.02 (d, *J* = 4.4 Hz, 1H), 6.93–6.88 (m, 2H), 4.09–3.95 (m, 8H), 1.42 (t, *J* = 7.0 Hz, 3H); ¹³C NMR (100 MHz, DMSO-*d*₆) δ 160.2, 155.5, 151.9, 150.9, 150.64, 150.62, 148.9, 146.0, 131.8, 123.8, 122.6, 122.5, 114.8, 113.4, 111.9, 109.0, 97.2, 63.6, 56.18, 56.17, 15.2; MS-ESI *m/z* 419 [MH⁺]; HRMS-FD calcd for C₂₃H₂₂N₄O₄ (M⁺) *m/z* = 418.16356; found, 418.16315; mp 157.1 °C; HPLC purity: 99.90%.

7-(3,4-Dimethoxyphenyl)-*N*-phenylpyrazolo[1,5-*a*]pyrimidine-2-carboxamide (5a). **4** (80 mg, 0.27 mmol), aniline (0.029 mL, 0.32 mmol), HBTU (152 mg, 0.40 mmol), and diisopropylethylamine (0.14 mL, 0.80 mmol) were combined in DCM (3 mL). After stirring for 24 h at r.t., the reaction mixture was extracted by DCM and aq NaHCO₃. The reaction mixture was purified by MPLC, elution gradient 20 to 50% EA in hexane. The crude mixture was solidified using EA and hexane to give **5a** (75.3 mg, 75%) as a white solid. ¹H NMR (400 MHz, DMSO-*d*₆) δ 10.24 (s, 1H), 8.69 (d, *J* = 4.5 Hz, 1H), 8.02 (dd, *J* = 8.5, 2.0 Hz, 1H), 7.96 (d, *J* = 2.0 Hz, 1H), 7.81 (d, *J* = 7.8 Hz, 2H), 7.49 (d, *J* = 4.5 Hz, 1H), 7.38 (t, *J* = 7.9 Hz, 2H), 7.30 (s, 1H), 7.22 (d, *J* = 8.6 Hz, 1H), 7.14 (t, *J* = 7.4 Hz, 1H), 3.93–3.87 (m, 6H); ¹³C NMR (100 MHz, DMSO-*d*₆) δ 160.6, 151.9, 151.0, 150.7, 150.4, 148.9, 146.1, 138.9, 129.2, 124.5, 123.8, 122.5, 120.9, 113.5, 111.9, 109.1, 97.3, 56.20, 56.18; MS-ESI *m/z* 375 [MH⁺]; HRMS-FD calcd for C₂₁H₁₈N₄O₃ (M⁺) *m/z* = 374.13734; found, 374.13745; mp 179.8 °C; HPLC purity: 99.62%.

Methyl 2-(7-(3,4-dimethoxyphenyl)pyrazolo[1,5-*a*]pyrimidine-2-carboxamido)benzoate (5b). **4** (80 mg, 0.27 mmol), methyl 2-aminobenzoate (0.042 mL, 0.32 mmol), HBTU (152 mg, 0.40 mmol), and diisopropylethylamine (0.14 mL, 0.80 mmol) were combined in DCM (3 mL). After stirring for 24 h at r.t., the reaction mixture was extracted by DCM and aq NaHCO₃. The reaction mixture was purified by MPLC, elution gradient 20 to 50% EA in hexane. The crude mixture was solidified using EA and hexane to give **5b** (44.4 mg, 38%) as a white solid. ¹H NMR (400 MHz, DMSO-*d*₆) δ 12.52 (s, 1H), 8.87 (d, *J* = 8.5 Hz, 1H), 8.72 (d, *J* = 4.5 Hz, 1H), 8.25 (dd, *J* = 8.5, 2.0 Hz, 1H), 8.09 (d, *J* = 7.8 Hz, 1H), 7.81 (d, *J* = 1.9 Hz, 1H), 7.73 (t, *J* = 7.8 Hz, 1H), 7.55 (d, *J* = 4.5 Hz, 1H), 7.31 (s, 1H), 7.29–7.21 (m, 2H), 3.95 (s, 3H), 3.92–3.89 (m, 6H); ¹³C NMR (100 MHz, DMSO-*d*₆) δ 168.1, 160.2, 152.0, 151.2, 151.1, 149.6, 149.0, 146.1, 140.8, 135.2, 131.4, 124.4, 123.6, 122.2, 120.3, 115.8, 113.0, 111.7, 109.4, 97.5, 56.2, 56.1, 52.9; MS-ESI *m/z* 433 [MH⁺]; HRMS-FD calcd for C₂₃H₂₀N₄O₅ (M⁺) *m/z* = 432.14282; found, 432.14303; mp 162.7 °C.

Methyl 3-(7-(3,4-dimethoxyphenyl)pyrazolo[1,5-*a*]pyrimidine-2-carboxamido)benzoate (5c). **4** (80 mg, 0.27 mmol), methyl 3-aminobenzoate (0.048 mL, 0.32 mmol), HBTU (152 mg, 0.40 mmol), and diisopropylethylamine (0.14 mL, 0.80 mmol) were combined in DCM (3 mL). After stirring for 24 h at r.t., the reaction mixture was extracted by DCM and aq NaHCO₃. The reaction mixture was purified by MPLC, elution gradient 50 to 65% EA in hexane. The crude mixture was solidified using EA and hexane to give **5c** (86.2 mg, 75%) as a white solid. ¹H NMR (400 MHz, DMSO-*d*₆) δ 10.52 (s, 1H), 8.70 (d, *J* = 4.5 Hz, 1H), 8.52 (s, 1H), 8.13–8.06 (m, 1H), 8.03 (dd, *J* = 8.5, 2.1 Hz, 1H), 7.95 (d, *J* = 2.0 Hz, 1H), 7.74 (d, *J* = 7.7 Hz, 1H), 7.54 (t, *J* = 7.9 Hz, 1H), 7.50 (d, *J* = 4.5 Hz, 1H), 7.33 (s, 1H), 7.23 (d, *J* = 8.6 Hz, 1H), 3.93–3.87 (m, 9H); ¹³C NMR (100 MHz, DMSO-*d*₆) δ 166.5, 160.9, 152.0, 151.0, 150.6, 150.1, 148.9, 146.1, 139.3, 130.6, 129.6, 125.5, 125.1, 123.8, 122.5, 121.5, 113.5, 111.9, 109.2, 97.5, 56.20, 56.17, 52.7; MS-ESI *m/z* 433 [MH⁺]; HRMS-FD calcd for C₂₃H₂₀N₄O₅ (M⁺) *m/z* = 432.14282; found, 432.14276; mp 179.3 °C; HPLC purity: 98.73%.

Methyl 4-(7-(3,4-dimethoxyphenyl)pyrazolo[1,5-*a*]pyrimidine-2-carboxamido)benzoate (5d). **4** (5000 mg, 16.71

mmol), methyl 4-aminobenzoate (2558 mg, 18.38 mmol), HBTU (6970 mg, 18.38 mmol), and diisopropylethylamine (5.82 mL, 33.41 mmol) were combined in DCM (167 mL). After stirring for 24 h at r.t., the reaction mixture was extracted by DCM and aq NaHCO₃. The reaction mixture was purified by MPLC, elution gradient 3 to 5% MeOH in DCM. The crude mixture was solidified using DCM and hexane to give **5d** (3501 mg, 48%) as a white solid. ¹H NMR (400 MHz, DMSO-*d*₆) δ 10.59 (s, 1H), 8.71 (d, *J* = 4.5 Hz, 1H), 8.05–7.94 (m, 6H), 7.51 (d, *J* = 4.5 Hz, 1H), 7.34 (s, 1H), 7.23 (d, *J* = 8.6 Hz, 1H), 3.93–3.89 (m, 6H), 3.85 (s, 3H); ¹³C NMR (100 MHz, DMSO-*d*₆) δ 166.3, 161.0, 152.0, 151.1, 150.7, 150.0, 148.9, 146.1, 143.4, 130.6, 125.1, 123.8, 122.5, 120.2, 113.5, 111.9, 109.2, 97.6, 56.21, 56.18, 52.4; MS-ESI *m/z* 433 [MH⁺]; HRMS-FD calcd for C₂₃H₂₀N₄O₅ (M⁺) *m/z* = 432.14282; found, 432.14287; mp 218.8 °C; HPLC purity: 99.51%.

7-(3,4-Dimethoxyphenyl)-*N*-(4-(2-morpholinoethoxy)phenyl)pyrazolo[1,5-*a*]pyrimidine-2-carboxamide (5e). **4** (1350 mg, 4.51 mmol), 4-(2-morpholinoethoxy)aniline (1203 mg, 5.41 mmol), HBTU (2566 mg, 6.77 mmol), and diisopropylethylamine (2.33 mL, 13.53 mmol) were combined in DCM (45 mL). After stirring for 24 h at r.t., the reaction mixture was extracted by DCM and aq NaHCO₃. The crude mixture was solidified using DCM and diethyl ether to give **5e** (1758 mg, 77%) as a yellow solid. ¹H NMR (400 MHz, DMSO-*d*₆) δ 10.13 (s, 1H), 8.68 (d, *J* = 4.5 Hz, 1H), 8.02 (dd, *J* = 8.5, 2.1 Hz, 1H), 7.94 (d, *J* = 2.1 Hz, 1H), 7.70 (d, *J* = 9.0 Hz, 2H), 7.48 (d, *J* = 4.5 Hz, 1H), 7.27 (s, 1H), 7.21 (d, *J* = 8.6 Hz, 1H), 6.96 (d, *J* = 9.1 Hz, 2H), 4.08 (t, *J* = 5.8 Hz, 2H), 3.94–3.86 (m, 6H), 3.63–3.54 (m, 4H), 2.69 (t, *J* = 5.8 Hz, 2H), 2.49–2.44 (m, 4H); ¹³C NMR (100 MHz, DMSO-*d*₆) δ 160.2, 155.4, 151.9, 150.9, 150.65, 150.61, 148.9, 146.1, 132.0, 123.8, 122.6, 114.9, 113.4, 111.9, 109.0, 97.2, 66.6, 65.9, 57.5, 56.20, 56.18, 54.1; MS-ESI *m/z* 504 [MH⁺]; HRMS-FD calcd for C₂₇H₂₉N₅O₅ (M⁺) *m/z* = 503.21632; found, 503.21613; mp 161.4 °C; HPLC purity: 98.33%.

7-(3,4-Dimethoxyphenyl)-*N*-(4-morpholinophenyl)pyrazolo[1,5-*a*]pyrimidine-2-carboxamide (5f). **4** (80 mg, 0.27 mmol), 4-morpholinoaniline (0.056 mL, 0.32 mmol), HBTU (152 mg, 0.40 mmol), and diisopropylethylamine (0.14 mL, 0.80 mmol) were combined in DCM (3 mL). After stirring for 24 h at r.t., the reaction mixture was extracted by DCM and aq NaHCO₃. The reaction mixture was purified by MPLC, elution gradient 50 to 65% EA in hexane. The crude mixture was solidified using EA and hexane to give **5f** (81.7 mg, 67%) as a gray solid. ¹H NMR (400 MHz, DMSO-*d*₆) δ 10.06 (s, 1H), 8.68 (d, *J* = 4.5 Hz, 1H), 8.02 (dd, *J* = 8.5, 2.0 Hz, 1H), 7.94 (d, *J* = 2.0 Hz, 1H), 7.66 (d, *J* = 9.0 Hz, 2H), 7.47 (d, *J* = 4.5 Hz, 1H), 7.26 (s, 1H), 7.21 (d, *J* = 8.6 Hz, 1H), 6.96 (d, *J* = 9.0 Hz, 2H), 3.97–3.82 (m, 6H), 3.82–3.70 (m, 4H), 3.13–2.97 (m, 4H); ¹³C NMR (100 MHz, DMSO-*d*₆) δ 160.0, 151.9, 150.9, 150.71, 150.66, 148.8, 148.2, 146.1, 131.0, 123.8, 122.6, 122.1, 115.7, 113.4, 111.9, 109.0, 97.2, 66.6, 56.19, 56.17, 49.2; MS-ESI *m/z* 460 [MH⁺]; HRMS-FD calcd for C₂₃H₂₃N₅O₄ (M⁺) *m/z* = 459.1011; found, 459.19031; mp 140.4 °C; HPLC purity: 99.54%.

Methyl 4-((7-(3,4-dimethoxyphenyl)pyrazolo[1,5-*a*]pyrimidine-2-carboxamido)methyl)benzoate (5g). **4** (80 mg, 0.27 mmol), methyl 4-(aminomethyl)benzoate hydrochloride (64.68 mg, 0.32 mmol), HBTU (152 mg, 0.40 mmol), and diisopropylethylamine (0.14 mL, 0.80 mmol) were combined in DCM (3 mL). After stirring for 24 h at r.t., the reaction mixture was extracted by DCM and aq NaHCO₃. The reaction mixture was purified by MPLC, elution gradient 20 to 50% EA in hexane. The crude mixture was solidified using EA and hexane to give **5g** (82.5 mg, 69%) as a white solid. ¹H NMR (400 MHz, DMSO-*d*₆) δ 9.09 (t, *J* = 6.3 Hz, 1H), 8.66 (dd, *J* = 4.5, 0.7 Hz, 1H), 7.97–7.90 (m, 3H), 7.86 (d, *J* = 1.4 Hz, 1H), 7.48 (d, *J* = 8.1 Hz, 2H), 7.44–7.41 (m, 1H), 7.21–7.15 (m, 2H), 4.60 (d, *J* = 6.2 Hz, 2H), 3.90–3.83 (m, 9H); ¹³C NMR (100 MHz, DMSO-*d*₆) δ 166.6, 161.9, 151.8, 150.8, 150.6, 150.1, 148.8, 146.1, 145.7, 129.7, 128.6, 127.8, 123.6, 122.6, 113.2, 111.9, 109.0, 97.0, 56.2, 56.0, 52.5, 42.5; MS-ESI *m/z* 447 [MH⁺]; HRMS-FD calcd for C₂₄H₂₂N₄O₅ (M⁺) *m/z* = 446.15847; found, 446.15827; mp 72.1 °C; HPLC purity: 98.02%.

7-(3,4-Dimethoxyphenyl)-*N*-(4-morpholinobenzyl)pyrazolo[1,5-*a*]pyrimidine-2-carboxamide (5h). **4** (80 mg, 0.27

mmol), (4-morpholinophenyl)methanamine (61.7 mg, 0.32 mmol), HBTU (152 mg, 0.40 mmol), and diisopropylethylamine (0.14 mL, 0.80 mmol) were combined in DCM (3 mL). After stirring for 24 h at r.t., the reaction mixture was extracted by DCM and aq NaHCO₃. The reaction mixture was purified by MPLC, elution gradient 20 to 50% EA in hexane. The crude mixture was solidified using EA and hexane to give **5h** (68.5 mg, 54%) as a beige solid. ¹H NMR (400 MHz, DMSO-*d*₆) δ 8.92–8.77 (m, 1H), 8.64 (d, *J* = 4.3 Hz, 1H), 7.92 (d, *J* = 7.6 Hz, 1H), 7.85 (s, 1H), 7.41 (d, *J* = 4.4 Hz, 1H), 7.33–7.06 (m, 4H), 6.89 (d, *J* = 8.4 Hz, 2H), 4.41 (d, *J* = 5.9 Hz, 2H), 3.89–3.82 (m, 6H), 3.80–3.67 (m, 4H), 3.17–2.98 (m, 4H); ¹³C NMR (100 MHz, DMSO-*d*₆) δ 161.6, 151.8, 150.8, 150.6, 150.4, 148.8, 146.0, 130.6, 128.7, 123.6, 122.6, 115.5, 113.2, 111.9, 108.9, 96.9, 66.5, 56.2, 56.0, 49.2, 42.2; MS-ESI *m/z* 474 [MH⁺]; HRMS-FD calcd for C₂₆H₂₇N₅O₄ (M⁺) *m/z* = 473.20576; found, 473.20623; mp 83.2 °C.

Methyl 4-(7-(3,4-dimethoxyphenyl)pyrazolo[1,5-*a*]pyrimidine-2-carboxamido)-3-fluorobenzoate (5i). To a solution of **4** (200 mg, 0.67 mmol) in DCM (6 mL), DMF (catalytic amount) and SOCl₂ (1 M, 3.34 mL) were added and stirred at 60 °C for 2 h. The mixture was concentrated and added dropwise to a solution of methyl 4-amino-3-fluorobenzoate (112.9 mg, 0.67 mmol) and pyridine (0.16 mL, 2.00 mmol) in DCM (6 mL) at 0 °C. After stirring for 1 h, the reaction mixture was extracted by DCM and aq NH₄Cl. The reaction mixture was purified by MPLC, elution gradient 5 to 9% MeOH in DCM. The crude mixture was solidified using DCM and hexane to give **5i** (70.5 mg, 23%) as a beige solid. ¹H NMR (400 MHz, DMSO-*d*₆) δ 10.00 (s, 1H), 8.72 (d, *J* = 4.5 Hz, 1H), 8.28 (t, *J* = 8.1 Hz, 1H), 7.95 (d, *J* = 2.1 Hz, 1H), 7.92–7.80 (m, 3H), 7.50 (d, *J* = 4.5 Hz, 1H), 7.34 (s, 1H), 7.21 (d, *J* = 8.6 Hz, 1H), 3.93–3.85 (m, 9H); ¹³C NMR (100 MHz, DMSO-*d*₆) δ 165.4, 160.3, 154.7, 152.2, 152.0, 151.4, 150.8, 149.0, 148.8, 146.2, 130.8, 130.7, 127.04, 126.97, 126.5, 126.4, 123.7, 123.6, 122.4, 116.7, 116.4, 113.2, 111.9, 109.6, 97.7, 56.2, 56.12, 56.10, 52.9; MS-ESI *m/z* 451 [MH⁺]; HRMS-FD calcd for C₂₃H₁₉FN₄O₅ (M⁺) *m/z* = 450.13340; found, 450.13344; mp 242.3 °C.

Methyl 3-Chloro-4-(7-(3,4-dimethoxyphenyl)pyrazolo[1,5-*a*]pyrimidine-2-carboxamido)benzoate (5j). To a solution of **4** (200 mg, 0.67 mmol) in DCM (6 mL), DMF (catalytic amount) and SOCl₂ (1 M, 3.34 mL) were added and stirred at 60 °C for 2 h. The mixture was concentrated and added dropwise to a solution of methyl 4-amino-3-chlorobenzoate (124.4 mg, 0.67 mmol) and pyridine (0.16 mL, 2.00 mmol) in DCM (6 mL) at 0 °C. After stirring for 1 h, the reaction mixture was extracted by DCM and aq NH₄Cl. The reaction mixture was purified by MPLC, elution gradient 5 to 9% MeOH in DCM. The crude mixture was solidified using DCM and hexane to give **5j** (236 mg, 76%) as a beige solid. ¹H NMR (400 MHz, CDCl₃) δ 9.92 (s, 1H), 8.81 (d, *J* = 8.7 Hz, 1H), 8.64 (d, *J* = 4.4 Hz, 1H), 8.13 (d, *J* = 1.9 Hz, 1H), 8.04 (dd, *J* = 8.6, 1.9 Hz, 1H), 7.78 (dd, *J* = 8.4, 2.1 Hz, 1H), 7.73 (d, *J* = 2.1 Hz, 1H), 7.45 (s, 1H), 7.12–7.07 (m, 2H), 4.04 (s, 3H), 4.01 (s, 3H), 3.95 (s, 3H); ¹³C NMR (100 MHz, CDCl₃) δ 165.7, 159.8, 152.0, 151.0, 150.2, 149.0, 148.8, 146.9, 138.4, 130.5, 129.5, 126.0, 123.3, 122.4, 122.3, 120.0, 112.3, 110.9, 108.7, 98.2, 56.3, 56.1, 52.3; MS-ESI *m/z* 467 [MH⁺]; HRMS-FD calcd for C₂₃H₁₉ClN₄O₅ (M⁺) *m/z* = 466.10385; found, 466.10440; mp 259.7 °C.

Methyl 4-(7-(3,4-dimethoxyphenyl)pyrazolo[1,5-*a*]pyrimidine-2-carboxamido)-3-methoxybenzoate (5k). To a solution of **4** (200 mg, 0.67 mmol) in DCM (6 mL), DMF (catalytic amount) and SOCl₂ (1 M, 3.34 mL) were added and stirred at 60 °C for 2 h. The mixture was concentrated and added dropwise to a solution of methyl 4-amino-3-methoxybenzoate (121.4 mg, 0.67 mmol) and pyridine (0.16 mL, 2.00 mmol) in DCM (6 mL) at 0 °C. After stirring for 1 h, the reaction mixture was extracted by DCM and aq NH₄Cl. The reaction mixture was purified by MPLC, elution gradient 5 to 9% MeOH in DCM. The crude mixture was solidified using DCM and hexane to give **5k** (220.0 mg, 71%) as an off-white solid. ¹H NMR (400 MHz, DMSO-*d*₆) δ 9.88 (s, 1H), 8.73 (d, *J* = 4.4 Hz, 1H), 8.54 (d, *J* = 8.4 Hz, 1H), 7.91 (d, *J* = 2.1 Hz, 1H), 7.81 (dd, *J* = 8.4, 2.1 Hz, 1H), 7.69 (dd, *J* = 8.4, 1.7 Hz, 1H), 7.59 (d, *J* = 1.7 Hz, 1H), 7.49 (d, *J* = 4.4 Hz, 1H), 7.31 (s, 1H), 7.26 (d, *J* = 8.6 Hz, 1H), 3.99–3.84 (m, 12H); ¹³C NMR (100 MHz, DMSO-*d*₆) δ 166.2, 159.5, 152.0, 151.4, 151.0, 148.9, 148.7, 148.0, 146.2, 131.7, 125.2, 123.6, 123.3, 122.4, 118.4, 113.3,

111.9, 111.3, 109.6, 97.3, 56.7, 56.3, 56.1, 52.6; MS-ESI *m/z* 463 [MH⁺]; HRMS-FD calcd for C₂₄H₂₂N₄O₆ (M⁺) *m/z* = 462.15339; found, 462.15350; mp 229.1 °C; HPLC purity: 96.54%.

Methyl 4-Amino-3-((tert-butylidimethylsilyloxy)benzoate (6). *tert*-Butylidimethylsilyl chloride (429 mg, 2.85 mmol) and imidazole (388 mg, 5.70 mmol) were combined in DCM (7.5 mL) at r.t.; then methyl 4-amino-3-hydroxybenzoate (500 mg, 2.99 mmol) solution in DCM (7.5 mL) was added dropwise. After stirring for 2.5 h, the reaction mixture was extracted by DCM and H₂O. The reaction mixture was purified by MPLC, elution gradient 10 to 25% EA in hexane to give **6** (722 mg, 90%) as a pale pink solid. ¹H NMR (400 MHz, DMSO-*d*₆) δ 7.37 (dd, *J* = 8.3, 1.9 Hz, 1H), 7.23 (d, *J* = 1.9 Hz, 1H), 6.70 (d, *J* = 8.3 Hz, 1H), 5.37 (s, 2H), 3.73 (s, 3H), 0.97 (s, 9H), 0.21 (s, 6H); MS-ESI *m/z* 282 [MH⁺].

Methyl 3-((tert-butylidimethylsilyloxy)-4-(7-(3,4-dimethoxyphenyl)pyrazolo[1,5-*a*]pyrimidine-2-carboxamido)benzoate (7). To a solution of **4** (100 mg, 0.33 mmol) in DCM (3 mL), DMF (catalytic amount) and SOCl₂ (1 M, 1.67 mL) were added and stirred at 60 °C for 2 h. The mixture was concentrated and added dropwise to a solution of **6** (93.9 mg, 0.33 mmol) and pyridine (0.08 mL, 1.00 mmol) in DCM (3 mL) at 0 °C. After stirring for 1 h, the reaction mixture was extracted by DCM and aq NH₄Cl. The reaction mixture was purified by MPLC, elution gradient 5 to 9% MeOH in DCM. The crude mixture was solidified using DCM and hexane to give **7** (131.2 mg, 23%) as a white solid. ¹H NMR (400 MHz, DMSO-*d*₆) δ 9.44 (s, 1H), 8.71 (d, *J* = 4.5 Hz, 1H), 8.48 (d, *J* = 8.5 Hz, 1H), 7.74–7.66 (m, 3H), 7.48–7.47 (m, 1H), 7.38 (d, *J* = 4.4 Hz, 1H), 7.32 (s, 1H), 7.20 (d, *J* = 8.5 Hz, 1H), 3.87 (s, 3H), 3.84 (s, 3H), 3.81 (s, 3H), 0.71 (s, 9H), 0.10 (s, 6H); MS-ESI *m/z* 563 [MH⁺].

Methyl 4-(7-(3,4-dimethoxyphenyl)pyrazolo[1,5-*a*]pyrimidine-2-carboxamido)-3-hydroxybenzoate (8). **7** (100 mg, 0.18 mmol) was dissolved in THF (2 mL) at 0 °C, followed by addition of tetrabutylammonium fluoride in THF (1 M, 0.18 mL). After stirring for 1 h, the reaction mixture was extracted by DCM and H₂O. The reaction mixture was purified by MPLC, elution gradient 2 to 5% MeOH in DCM to give **8** (43.9 mg, 55%) as a white solid. ¹H NMR (400 MHz, DMSO-*d*₆) δ 11.00 (s, 1H), 9.82 (s, 1H), 8.72 (d, *J* = 4.3 Hz, 1H), 8.48 (d, *J* = 8.3 Hz, 1H), 8.00 (s, 1H), 7.73 (d, *J* = 8.4 Hz, 1H), 7.57–7.38 (m, 3H), 7.31 (s, 1H), 7.21 (d, *J* = 8.4 Hz, 1H), 3.95–3.85 (m, 6H), 3.82 (s, 3H); ¹³C NMR (100 MHz, DMSO-*d*₆) δ 166.3, 159.4, 151.9, 151.4, 151.0, 149.2, 148.6, 146.4, 146.3, 131.0, 125.2, 123.5, 122.5, 121.6, 118.7, 115.2, 113.0, 112.0, 109.7, 97.4, 56.2, 56.0, 52.5; MS-ESI *m/z* 449 [MH⁺]; HRMS-FD calcd for C₂₃H₂₀N₄O₆ (M⁺) *m/z* = 448.13774; found, 448.13770; mp 253.1 °C.

4-(7-(3,4-Dimethoxyphenyl)pyrazolo[1,5-*a*]pyrimidine-2-carboxamido)benzoic Acid (9a). **5d** (2260 mg, 5.23 mmol) was dissolved in H₂O/THF/MeOH (21/34/17 mL), followed by addition of sodium hydroxide in H₂O (1 N, 10.5 mL) and stirred at 60 °C for 2 h. After cooling at 0 °C, the mixture was acidified by adding 1 N HCl. Then the precipitated crystals were filtered out by using H₂O to give **9a** (2920 mg, >99%) as a yellow solid. ¹H NMR (400 MHz, DMSO-*d*₆) δ 12.72 (s, 1H), 10.53 (s, 1H), 8.71 (d, *J* = 4.1 Hz, 1H), 8.09–7.84 (m, 6H), 7.50 (d, *J* = 4.3 Hz, 1H), 7.34 (s, 1H), 7.23 (d, *J* = 8.4 Hz, 1H), 4.00–3.82 (m, 6H); ¹³C NMR (100 MHz, DMSO-*d*₆) δ 167.4, 161.0, 152.0, 151.1, 150.7, 150.1, 148.9, 146.1, 143.0, 130.7, 126.3, 123.8, 122.5, 120.1, 113.5, 111.9, 109.2, 97.6, 56.21, 56.19; MS-ESI *m/z* 419 [MH⁺]; HRMS-FD calcd for C₂₂H₁₈N₄O₅ (M⁺) *m/z* = 418.12717; found, 418.12753; mp 253.8 °C.

4-(7-(3,4-Dimethoxyphenyl)pyrazolo[1,5-*a*]pyrimidine-2-carboxamido)-3-fluorobenzoic Acid (9b). **5i** (30 mg, 0.067 mmol) was dissolved in H₂O/THF/MeOH (0.3/0.8/0.4 mL), followed by addition of sodium hydroxide in H₂O (1 N, 0.13 mL) and stirred at 60 °C for 2 h. After cooling at 0 °C, the mixture was acidified by adding 1 N HCl. Then the precipitated crystals were filtered out by using H₂O to give **9b** (24.6 mg, 85%) as an orange solid. ¹H NMR (400 MHz, DMSO-*d*₆) δ 9.97 (s, 1H), 8.72 (d, *J* = 4.5 Hz, 1H), 8.20 (t, *J* = 8.1 Hz, 1H), 7.95 (d, *J* = 2.0 Hz, 1H), 7.90 (dd, *J* = 8.4, 2.0 Hz, 1H), 7.86–7.82 (m, 1H), 7.78 (dd, *J* = 11.3, 1.6 Hz, 1H), 7.50 (d, *J* = 4.5 Hz, 1H), 7.34 (s, 1H), 7.22 (d, *J* = 8.6 Hz, 1H), 3.93–3.88 (m, 6H); ¹³C NMR (100 MHz, DMSO-*d*₆) δ 166.42, 166.40, 160.2, 154.7, 152.3, 152.0, 151.3,

150.8, 149.0, 148.8, 146.2, 130.3, 130.2, 128.43, 128.36, 126.50, 126.48, 123.7, 123.6, 122.4, 116.7, 116.5, 113.2, 111.9, 109.6, 97.7, 56.2, 56.12, 56.10; MS-ESI m/z 437 [MH⁺]; HRMS-FD calcd for C₂₂H₁₇FN₄O₅ (M⁺) m/z = 436.11775; found, 436.11742; mp 239.5 °C.

7-(3,4-Dimethoxyphenyl)-N-(4-(morpholine-4-carbonyl)-phenyl)pyrazolo[1,5-*a*]pyrimidine-2-carboxamide (10a). **9a** (80 mg, 0.19 mmol), morpholine (0.019 mL, 0.23 mmol), HBTU (109 mg, 0.29 mmol), and diisopropylethylamine (0.10 mL, 0.57 mmol) were combined in DCM (2 mL). After stirring for 24 h at r.t., the reaction mixture was extracted by DCM and aq NaHCO₃. The reaction mixture was purified by MPLC, elution gradient 2 to 5% MeOH in DCM. The crude mixture was solidified using EA and hexane to give **10a** (58.0 mg, 62%) as an off-white solid. ¹H NMR (400 MHz, DMSO-*d*₆) δ 10.43 (s, 1H), 8.70 (d, *J* = 4.5 Hz, 1H), 8.01 (dd, *J* = 8.5, 2.1 Hz, 1H), 7.96 (d, *J* = 2.0 Hz, 1H), 7.90 (d, *J* = 8.5 Hz, 2H), 7.49 (d, *J* = 4.5 Hz, 1H), 7.45 (d, *J* = 8.5 Hz, 2H), 7.32 (s, 1H), 7.22 (d, *J* = 8.6 Hz, 1H), 3.93–3.87 (m, 6H), 3.67–3.39 (m, 8H); ¹³C NMR (100 MHz, DMSO-*d*₆) δ 169.3, 160.8, 152.0, 151.1, 150.7, 150.2, 148.9, 146.1, 140.2, 131.2, 128.5, 123.8, 122.5, 120.4, 113.5, 111.9, 109.2, 97.5, 66.6, 56.21, 56.18, 54.1; MS-ESI m/z 488 [MH⁺]; HRMS-FD calcd for C₂₆H₂₅N₅O₅ (M⁺) m/z = 487.18502; found, 487.18513; mp 240.6 °C; HPLC purity: 99.48%.

tert-Butyl 4-(4-(7-(3,4-dimethoxyphenyl)pyrazolo[1,5-*a*]pyrimidine-2-carboxamido)benzoyl)piperazine-1-carboxylate (10b). **9a** (80 mg, 0.19 mmol), *tert*-butyl piperazine-1-carboxylate (42.7 mg, 0.23 mmol), HBTU (109 mg, 0.29 mmol), and diisopropylethylamine (0.10 mL, 0.57 mmol) were combined in DCM (2 mL). After stirring for 24 h at r.t., the reaction mixture was extracted by DCM and aq NaHCO₃. The reaction mixture was purified by MPLC, elution gradient 2 to 5% MeOH in DCM, to give **10b** (109 mg, 97%) as an off-white solid. ¹H NMR (400 MHz, DMSO-*d*₆) δ 10.45 (s, 1H), 8.70 (d, *J* = 4.5 Hz, 1H), 8.02 (dd, *J* = 8.5, 2.1 Hz, 1H), 7.96 (d, *J* = 2.1 Hz, 1H), 7.90 (d, *J* = 8.6 Hz, 2H), 7.50 (d, *J* = 4.5 Hz, 1H), 7.45 (d, *J* = 8.6 Hz, 2H), 7.32 (s, 1H), 7.22 (d, *J* = 8.6 Hz, 1H), 3.92–3.88 (m, 6H), 3.61–3.35 (m, 8H), 1.41 (s, 9H); ¹³C NMR (100 MHz, DMSO-*d*₆) δ 169.4, 160.8, 154.3, 151.9, 151.1, 150.7, 150.2, 148.8, 146.1, 140.2, 131.3, 128.5, 123.8, 122.5, 120.3, 113.4, 111.9, 109.2, 97.5, 79.7, 56.20, 56.17, 55.4, 28.5; MS-ESI m/z 587 [MH⁺]; HRMS-FD calcd for C₃₁H₃₄N₆O₆ (M⁺) m/z = 586.25343; found, 586.25324; mp 154.3 °C; HPLC purity: 98.09%.

tert-Butyl 2-(4-(7-(3,4-dimethoxyphenyl)pyrazolo[1,5-*a*]pyrimidine-2-carboxamido)benzamide)ethyl)carbamate (10c). **9a** (80 mg, 0.19 mmol), *tert*-butyl *N*-(2-aminoethyl)carbamate (0.036 mL, 0.23 mmol), HBTU (109 mg, 0.29 mmol), and diisopropylethylamine (0.10 mL, 0.57 mmol) were combined in DCM (2 mL). After stirring for 24 h at r.t., the reaction mixture was extracted by DCM and aq NaHCO₃. The reaction mixture was purified by MPLC, elution gradient 2 to 5% MeOH in DCM. The crude mixture was solidified using DCM and hexane to give **10c** (76.3 mg, 71%) as a yellow solid. ¹H NMR (400 MHz, DMSO-*d*₆) δ 10.45 (s, 1H), 8.70 (d, *J* = 4.5 Hz, 1H), 8.40 (t, *J* = 5.5 Hz, 1H), 8.02 (dd, *J* = 8.5, 2.1 Hz, 1H), 7.96 (d, *J* = 2.1 Hz, 1H), 7.94–7.82 (m, 4H), 7.50 (d, *J* = 4.5 Hz, 1H), 7.33 (s, 1H), 7.23 (d, *J* = 8.6 Hz, 1H), 6.92 (t, *J* = 5.5 Hz, 1H), 3.93–3.86 (m, 6H), 3.31–3.25 (m, 2H), 3.15–3.07 (m, 2H), 1.39 (s, 9H); ¹³C NMR (100 MHz, DMSO-*d*₆) δ 166.3, 160.8, 156.2, 151.9, 151.1, 150.7, 150.2, 148.8, 146.1, 141.4, 130.2, 128.4, 123.8, 122.5, 120.0, 113.4, 111.9, 109.2, 97.5, 78.2, 56.2, 56.1, 28.7; MS-ESI m/z 583 [MNa⁺]; HRMS-FD calcd for C₂₉H₃₂N₆O₆ (M⁺) m/z = 560.23778; found, 560.23779; mp 183.0 °C; HPLC purity: 98.66%.

7-(3,4-Dimethoxyphenyl)-N-(4-(4-methylpiperazine-1-carbonyl)phenyl)pyrazolo[1,5-*a*]pyrimidine-2-carboxamide (10d). **9a** (80 mg, 0.19 mmol), 1-methylpiperazine (0.025 mL, 0.23 mmol), HBTU (109 mg, 0.29 mmol), and diisopropylethylamine (0.10 mL, 0.57 mmol) were combined in DCM (2 mL). After stirring for 24 h at r.t., the reaction mixture was extracted by DCM and aq NaHCO₃. The reaction mixture was purified by MPLC, elution gradient 2 to 5% MeOH in DCM. The crude mixture was solidified using DCM and hexane to give **10d** (77.0 mg, 80%) as a pale-yellow solid. ¹H NMR (400 MHz, DMSO-*d*₆) δ 10.44 (s, 1H), 8.70 (d, *J* = 4.5 Hz, 1H), 8.02 (dd, *J* = 8.5, 2.1 Hz, 1H), 7.96 (d, *J* = 2.1 Hz, 1H), 7.90 (d, *J* = 8.6 Hz, 2H), 7.50 (d, *J* = 4.5 Hz, 1H), 7.43 (d, *J* = 8.6 Hz, 2H), 7.32 (s, 1H),

7.22 (d, *J* = 8.6 Hz, 1H), 3.94–3.85 (m, 6H), 3.68–3.37 (m, 4H), 2.44–2.27 (m, 4H), 2.22 (s, 3H); MS-ESI m/z 501 [MH⁺].

7-(3,4-Dimethoxyphenyl)-N-(4-(piperazine-1-carbonyl)-phenyl)pyrazolo[1,5-*a*]pyrimidine-2-carboxamide Hydrochloride (11a). **10b** (50 mg, 0.085 mmol) was dissolved in MeOH (1 mL), followed by addition of hydrogen chloride in dioxane (4 N, 0.21 mL) and stirring at r.t. for 26 h. The crude mixture was solidified using acetone to give **11a** (25.5 mg, 57%) as an orange solid. ¹H NMR (400 MHz, DMSO-*d*₆) δ 10.49 (s, 1H), 9.46 (s, 2H), 8.70 (d, *J* = 4.5 Hz, 1H), 8.01 (dd, *J* = 8.5, 2.1 Hz, 1H), 7.96 (d, *J* = 2.1 Hz, 1H), 7.93 (d, *J* = 8.7 Hz, 2H), 7.53–7.48 (m, 3H), 7.35 (s, 1H), 7.22 (d, *J* = 8.6 Hz, 1H), 3.92–3.86 (m, 6H), 3.81–3.64 (m, 4H), 3.21–3.09 (m, 4H); ¹³C NMR (100 MHz, DMSO-*d*₆) δ 169.5, 160.9, 151.9, 151.1, 150.6, 150.2, 148.8, 146.1, 140.5, 130.4, 128.7, 123.8, 122.5, 120.4, 113.4, 111.9, 109.2, 97.6, 56.20, 56.15, 42.9; MS-ESI m/z 487 [MH⁺]; HRMS-FD calcd for C₂₆H₂₆N₆O₄ (M⁺) m/z = 486.17768; found, 486.17794; mp 69.3 °C; HPLC purity: 95.80%.

N-(4-((2-Aminoethyl)carbamoyl)phenyl)-7-(3,4-dimethoxyphenyl)pyrazolo[1,5-*a*]pyrimidine-2-carboxamide Hydrochloride (11b). **10c** (40 mg, 0.071 mmol) was dissolved in MeOH (1 mL), followed by addition of hydrogen chloride in dioxane (4 N, 0.18 mL) and stirring at r.t. for 26 h. The crude mixture was solidified using acetone to give **11b** (26.9 mg, 76%) as an orange solid. ¹H NMR (400 MHz, DMSO-*d*₆) δ 10.50 (s, 1H), 8.73–8.64 (m, 2H), 8.13–7.85 (m, 9H), 7.51 (d, *J* = 4.5 Hz, 1H), 7.34 (s, 1H), 7.23 (d, *J* = 8.6 Hz, 1H), 3.93–3.87 (m, 6H), 3.56–3.49 (m, 2H), 3.04–2.96 (m, 2H); ¹³C NMR (100 MHz, DMSO-*d*₆) δ 166.7, 160.9, 151.9, 151.1, 150.6, 150.1, 148.8, 146.1, 141.7, 129.6, 128.7, 123.8, 122.5, 120.0, 113.4, 111.9, 109.2, 97.6, 56.22, 56.17, 39.1, 37.6; MS-ESI m/z 461 [MH⁺]; HRMS-FD calcd for C₂₄H₂₄N₆O₄ (M⁺) m/z = 460.16203; found, 460.16260; mp 213.0 °C; HPLC purity: 98.71%.

7-(3,4-Dimethoxyphenyl)-N-(4-(4-methylpiperazine-1-carbonyl)phenyl)pyrazolo[1,5-*a*]pyrimidine-2-carboxamide Hydrochloride (11c). **10d** (40 mg, 0.080 mmol) was dissolved in MeOH (1 mL), followed by addition of hydrogen chloride in dioxane (4 N, 0.20 mL) and stirring at r.t. for 26 h. The crude mixture was solidified using acetone to give **11c** (24.7 mg, 58%) as an orange solid. ¹H NMR (400 MHz, DMSO-*d*₆) δ 11.18 (s, 1H), 10.53 (s, 1H), 8.70 (s, 1H), 8.05–7.89 (m, 4H), 7.55–7.46 (m, 3H), 7.35 (s, 1H), 7.22 (d, *J* = 8.5 Hz, 1H), 3.95–3.86 (m, 6H), 3.63–2.89 (m, 8H), 2.77 (s, 3H); ¹³C NMR (100 MHz, DMSO-*d*₆) δ 169.4, 160.9, 151.9, 151.1, 150.7, 150.1, 148.8, 146.1, 140.6, 130.2, 128.7, 123.8, 122.5, 120.4, 113.4, 111.9, 109.2, 97.6, 56.23, 56.18, 52.4, 42.5; MS-ESI m/z 501 [MH⁺]; HRMS-FD calcd for C₂₇H₂₈N₆O₄ (M⁺) m/z = 500.21665; found, 500.21600; mp 74.2 °C.

N-Cyclohexyl-7-(3,4-dimethoxyphenyl)pyrazolo[1,5-*a*]pyrimidine-2-carboxamide (12a). **4** (80 mg, 0.27 mmol), cyclohexylamine (0.037 mL, 0.32 mmol), HBTU (152 mg, 0.40 mmol), and diisopropylethylamine (0.14 mL, 0.80 mmol) were combined in DCM (3 mL). After stirring for 24 h at r.t., the reaction mixture was extracted by DCM and aq NaHCO₃. The reaction mixture was purified by MPLC, elution gradient 20 to 50% EA in hexane. The crude mixture was solidified using EA and hexane to give **12a** (54.6 mg, 54%) as a yellow solid. ¹H NMR (400 MHz, DMSO-*d*₆) δ 8.64 (d, *J* = 4.5 Hz, 1H), 8.05 (d, *J* = 8.3 Hz, 1H), 7.97 (d, *J* = 2.1 Hz, 1H), 7.89 (dd, *J* = 8.5, 2.1 Hz, 1H), 7.42 (d, *J* = 4.5 Hz, 1H), 7.20 (d, *J* = 8.6 Hz, 1H), 7.13 (s, 1H), 3.90–3.88 (m, 6H), 3.85–3.76 (m, 1H), 1.90–1.68 (m, 4H), 1.66–1.55 (m, 1H), 1.45–1.24 (m, 4H), 1.21–1.07 (m, 1H); ¹³C NMR (100 MHz, DMSO-*d*₆) δ 160.8, 151.8, 150.7, 150.62, 150.58, 148.7, 145.9, 123.5, 122.6, 113.4, 111.9, 108.7, 96.7, 56.2, 56.0, 48.4, 32.7, 25.6, 25.3; MS-ESI m/z 381 [MH⁺]; HRMS-FD calcd for C₂₁H₂₄N₄O₃ (M⁺) m/z = 380.18429; found, 380.18449; mp 157.4 °C; HPLC purity: 99.61%.

Methyl (1s,4s)-4-(7-(3,4-dimethoxyphenyl)pyrazolo[1,5-*a*]pyrimidine-2-carboxamido)cyclohexane-1-carboxylate (12b). **4** (150 mg, 0.50 mmol), methyl *cis*-4-aminocyclohexanecarboxylate hydrochloride (116.5 mg, 0.60 mmol), HBTU (285 mg, 0.75 mmol), and diisopropylethylamine (0.26 mL, 1.50 mmol) were combined in DCM (5 mL). After stirring for 24 h at r.t., the reaction mixture was extracted by DCM and aq NaHCO₃. The reaction mixture was purified

by MPLC, elution gradient 50 to 75% EA in hexane. The crude mixture was solidified using EA and hexane to give **12b** (98.1 mg, 45%) as a yellow solid. ¹H NMR (400 MHz, DMSO-*d*₆) δ 8.64 (d, *J* = 4.5 Hz, 1H), 8.07 (d, *J* = 7.9 Hz, 1H), 7.98 (d, *J* = 2.1 Hz, 1H), 7.90 (dd, *J* = 8.5, 2.1 Hz, 1H), 7.43 (d, *J* = 4.5 Hz, 1H), 7.20 (d, *J* = 8.6 Hz, 1H), 7.14 (s, 1H), 3.99–3.86 (m, 7H), 3.64 (s, 3H), 2.65–2.57 (m, 1H), 2.01–1.88 (m, 2H), 1.74–1.56 (m, 6H); ¹³C NMR (100 MHz, DMSO-*d*₆) δ 175.1, 161.1, 151.8, 150.7, 150.6, 150.5, 148.7, 145.9, 123.6, 122.6, 113.4, 111.9, 108.7, 96.7, 56.2, 56.1, 51.9, 46.8, 39.3, 29.2, 25.6; MS-ESI *m/z* 439 [MH⁺]; HRMS-FD calcd for C₂₃H₂₆N₄O₅ (M⁺) *m/z* = 438.18977; found, 438.18971; HPLC purity: 98.45%.

Methyl (1*r*,4*r*)-4-(7-(3,4-dimethoxyphenyl)pyrazolo[1,5-*a*]pyrimidine-2-carboxamido)cyclohexane-1-carboxylate (12c). **4** (500 mg, 1.67 mmol), methyl *trans*-4-aminocyclohexanecarboxylate hydrochloride (356 mg, 1.84 mmol), HBTU (698 mg, 1.84 mmol), and diisopropylethylamine (1.44 mL, 8.35 mmol) were combined in DCM (17 mL). After stirring for 24 h at r.t., the reaction mixture was extracted by DCM and aq NaHCO₃. The reaction mixture was purified by MPLC, elution gradient 50 to 75% EA in hexane. The crude mixture was solidified using EA and hexane to give **12c** (511.2 mg, 70%) as a yellow solid. ¹H NMR (400 MHz, DMSO-*d*₆) δ 8.64 (d, *J* = 4.5 Hz, 1H), 8.10 (d, *J* = 8.3 Hz, 1H), 7.96 (d, *J* = 2.1 Hz, 1H), 7.90 (dd, *J* = 8.5, 2.1 Hz, 1H), 7.42 (d, *J* = 4.5 Hz, 1H), 7.20 (d, *J* = 8.6 Hz, 1H), 7.13 (s, 1H), 3.91–3.88 (m, 6H), 3.86–3.74 (m, 1H), 3.61 (s, 3H), 2.35–2.24 (m, 1H), 2.01–1.83 (m, 4H), 1.52–1.35 (m, 4H); ¹³C NMR (100 MHz, DMSO-*d*₆) δ 175.6, 161.0, 151.8, 150.7, 150.6, 150.5, 148.7, 145.9, 123.5, 122.6, 113.4, 111.9, 108.8, 96.8, 56.2, 56.0, 51.8, 47.9, 42.0, 31.4, 28.1; MS-ESI *m/z* 439 [MH⁺]; HRMS-FD calcd for C₂₃H₂₆N₄O₅ (M⁺) *m/z* = 438.18977; found, 438.18981; mp 150.8 °C; HPLC purity: 99.96%.

Methyl 3-(7-(3,4-dimethoxyphenyl)pyrazolo[1,5-*a*]pyrimidine-2-carboxamido)bicyclo[1.1.1]pentane-1-carboxylate (12d). **4** (180 mg, 0.60 mmol), methyl 3-aminobicyclo[1.1.1]pentane-1-carboxylate hydrochloride (128.2 mg, 0.72 mmol), HBTU (342 mg, 0.90 mmol), and diisopropylethylamine (0.31 mL, 1.80 mmol) were combined in DCM (6 mL). After stirring for 24 h at r.t., the reaction mixture was extracted by DCM and aq NaHCO₃. The reaction mixture was purified by MPLC, elution gradient 20 to 50% EA in hexane, to give **12d** (252 mg, 99%) as a yellow solid. ¹H NMR (400 MHz, DMSO-*d*₆) δ 9.08 (s, 1H), 8.64 (d, *J* = 4.5 Hz, 1H), 7.97 (dd, *J* = 8.5, 2.1 Hz, 1H), 7.80 (d, *J* = 2.0 Hz, 1H), 7.42 (d, *J* = 4.5 Hz, 1H), 7.19 (d, *J* = 8.6 Hz, 1H), 7.12 (s, 1H), 3.91–3.86 (m, 6H), 3.63 (s, 3H), 2.36 (s, 6H); ¹³C NMR (100 MHz, DMSO-*d*₆) δ 169.8, 162.3, 151.9, 150.8, 150.5, 150.2, 148.9, 146.1, 123.7, 122.5, 113.3, 111.9, 109.0, 96.9, 56.2, 56.1, 54.6, 52.0, 46.1, 36.3; MS-ESI *m/z* 423 [MH⁺]; HRMS-FD calcd for C₂₂H₂₂N₄O₅ (M⁺) *m/z* = 422.15847; found, 422.15810; mp 148.6 °C; HPLC purity: 99.40%.

(1*s*,4*s*)-4-(7-(3,4-Dimethoxyphenyl)pyrazolo[1,5-*a*]pyrimidine-2-carboxamido)cyclohexane-1-carboxylic Acid (13a). **12b** (55 mg, 0.13 mmol) was dissolved in H₂O/THF/MeOH (1/0.8/0.4 mL), followed by addition of sodium hydroxide in H₂O (1 N, 0.25 mL) and stirring at 60 °C for 2 h. After cooling at 0 °C, the mixture was acidified by adding 1 N HCl. Then the precipitated crystals were filtered out by using H₂O to give **13a** (40.4 mg, 76%) as a yellow solid. ¹H NMR (400 MHz, DMSO-*d*₆) δ 8.64 (d, *J* = 4.5 Hz, 1H), 8.08 (d, *J* = 7.7 Hz, 1H), 7.98 (d, *J* = 2.0 Hz, 1H), 7.94–7.88 (m, 1H), 7.43 (d, *J* = 4.5 Hz, 1H), 7.21 (s, 1H), 7.14 (s, 1H), 3.94–3.86 (m, 7H), 2.48–2.43 (m, 1H), 1.99–1.90 (m, 2H), 1.72–1.57 (m, 6H); ¹³C NMR (100 MHz, DMSO-*d*₆) δ 176.4, 161.0, 151.8, 150.7, 150.6, 150.5, 148.7, 145.9, 123.6, 122.6, 113.4, 111.9, 108.7, 96.7, 56.2, 56.1, 47.0, 39.3, 29.3, 25.6; MS-ESI *m/z* 425 [MH⁺]; HRMS-FD calcd for C₂₂H₂₄N₄O₅ (M⁺) *m/z* = 424.17412; found, 424.17390; mp 234.6 °C; HPLC purity: 96.67%.

(1*r*,4*r*)-4-(7-(3,4-Dimethoxyphenyl)pyrazolo[1,5-*a*]pyrimidine-2-carboxamido)cyclohexane-1-carboxylic Acid (13b). **12c** (1420 mg, 3.23 mmol) was dissolved in H₂O/THF/MeOH (12/22/11 mL), followed by addition of sodium hydroxide in H₂O (1 N, 6.46 mL) and stirring at 60 °C for 2 h. After cooling at 0 °C, the mixture was acidified by adding 1 N HCl. Then the precipitated crystals were filtered out by using H₂O to give **13b** (1099 mg, 80%) as a

pale-yellow solid. ¹H NMR (400 MHz, DMSO-*d*₆) δ 12.06 (s, 1H), 8.64 (d, *J* = 4.5 Hz, 1H), 8.10 (d, *J* = 8.3 Hz, 1H), 7.96 (d, *J* = 2.1 Hz, 1H), 7.90 (dd, *J* = 8.5, 2.1 Hz, 1H), 7.43 (d, *J* = 4.5 Hz, 1H), 7.20 (d, *J* = 8.6 Hz, 1H), 7.13 (s, 1H), 3.92–3.87 (m, 6H), 3.82–3.73 (m, 1H), 2.22–2.12 (m, 1H), 2.02–1.85 (m, 4H), 1.52–1.35 (m, 4H); ¹³C NMR (100 MHz, DMSO-*d*₆) δ 176.9, 161.0, 151.8, 150.7, 150.6, 150.5, 148.7, 145.9, 123.5, 122.6, 113.4, 111.9, 108.8, 96.8, 56.2, 56.0, 48.0, 42.2, 31.6, 28.2; MS-ESI *m/z* 425 [MH⁺]; HRMS-FD calcd for C₂₂H₂₄N₄O₅ (M⁺) *m/z* = 424.17412; found, 424.17419; mp 258.9 °C; HPLC purity: 96.35%.

3-(7-(3,4-Dimethoxyphenyl)pyrazolo[1,5-*a*]pyrimidine-2-carboxamido)bicyclo[1.1.1]pentane-1-carboxylic Acid (13c). **12d** (100 mg, 0.24 mmol) was dissolved in H₂O/THF/MeOH (1/1.6/0.8 mL), followed by addition of sodium hydroxide in H₂O (1 N, 0.48 mL) and stirring at 60 °C for 2 h. After cooling at 0 °C, the mixture was acidified by adding 1 N HCl. The reaction mixture was extracted by DCM and H₂O. The crude mixture was solidified using DCM and hexane to give **13c** (74.5 mg, 77%) as a yellow solid. ¹H NMR (400 MHz, DMSO-*d*₆) δ 12.49 (s, 1H), 9.03 (s, 1H), 8.64 (d, *J* = 4.5 Hz, 1H), 7.97 (dd, *J* = 8.5, 2.1 Hz, 1H), 7.80 (d, *J* = 2.1 Hz, 1H), 7.42 (d, *J* = 4.5 Hz, 1H), 7.19 (d, *J* = 8.6 Hz, 1H), 7.12 (s, 1H), 3.93–3.87 (m, 6H), 2.32 (s, 6H); ¹³C NMR (100 MHz, DMSO-*d*₆) δ 171.2, 162.3, 151.8, 150.8, 150.5, 150.2, 148.9, 146.1, 123.7, 122.5, 113.3, 111.9, 109.0, 96.9, 56.2, 56.1, 54.4, 45.9, 36.6; MS-ESI *m/z* 409 [MH⁺]; HRMS-FD calcd for C₂₁H₂₀N₄O₅ (M⁺) *m/z* = 408.14282; found, 418.14275; mp 235.7 °C; HPLC purity: 98.94%.

***tert*-Butyl (1-(7-(3,4-dimethoxyphenyl)pyrazolo[1,5-*a*]pyrimidine-2-carboxamido)azetidino-3-yl)carbamate (14a).** **4** (60 mg, 0.20 mmol), *tert*-butyl *N*-(azetidino-3-yl)carbamate (38 mg, 0.22 mmol), HBTU (114 mg, 0.30 mmol), and diisopropylethylamine (0.10 mL, 0.60 mmol) were combined in DCM (2 mL). After stirring for 24 h at r.t., the reaction mixture was extracted by DCM and aq NaHCO₃. The reaction mixture was purified by MPLC, elution gradient 2 to 5% MeOH in DCM. The crude mixture was solidified using DCM and hexane to give **14a** (30 mg, 33%) as a yellow solid. ¹H NMR (400 MHz, DMSO-*d*₆) δ 8.66 (d, *J* = 4.4 Hz, 1H), 7.82 (dd, *J* = 8.3, 1.7 Hz, 1H), 7.74 (d, *J* = 1.4 Hz, 1H), 7.65 (d, *J* = 6.5 Hz, 1H), 7.40 (d, *J* = 4.4 Hz, 1H), 7.20 (d, *J* = 8.6 Hz, 1H), 7.10 (s, 1H), 4.89–4.68 (m, 1H), 4.46–4.26 (m, 3H), 3.95–3.82 (m, 7H), 1.39 (s, 9H); ¹³C NMR (100 MHz, DMSO-*d*₆) δ 161.5, 155.3, 151.9, 151.0, 149.92, 149.89, 148.8, 146.2, 123.6, 122.7, 113.1, 111.8, 109.2, 97.8, 78.8, 60.9, 56.20, 56.16, 55.7, 28.6; MS-ESI *m/z* 454 [MH⁺]; HRMS-FD calcd for C₂₃H₂₇N₅O₅ (M⁺) *m/z* = 453.20067; found, 453.20071; mp 123.8 °C; HPLC purity: 99.90%.

***tert*-Butyl (R)-(1-(7-(3,4-dimethoxyphenyl)pyrazolo[1,5-*a*]pyrimidine-2-carboxamido)pyrrolidin-3-yl)carbamate (14b).** **4** (60 mg, 0.20 mmol), *tert*-butyl *N*-[(3*R*)-pyrrolidin-3-yl]carbamate (41 mg, 0.22 mmol), HBTU (114 mg, 0.30 mmol), and diisopropylethylamine (0.10 mL, 0.60 mmol) were combined in DCM (2 mL). After stirring for 24 h at r.t., the reaction mixture was extracted by DCM and aq NaHCO₃. The reaction mixture was purified by MPLC, elution gradient 2 to 5% MeOH in DCM. The crude mixture was solidified using DCM and hexane to give **14b** (44.6 mg, 48%) as a yellow solid. ¹H NMR (400 MHz, DMSO-*d*₆) δ 8.65 (dd, *J* = 4.4, 1.2 Hz, 1H), 7.86–7.76 (m, 2H), 7.38 (dd, *J* = 4.4, 1.2 Hz, 1H), 7.29–7.15 (m, 2H), 7.09 (d, *J* = 3.8 Hz, 1H), 4.13–3.95 (m, 2H), 3.90–3.82 (m, 6H), 3.77–3.37 (m, 3H), 2.16–1.97 (m, 1H), 1.89–1.74 (m, 1H), 1.46–1.28 (m, 9H); ¹³C NMR (100 MHz, DMSO-*d*₆) δ 161.6, 155.7, 152.5, 151.7, 150.7, 150.0, 149.4, 146.2, 123.7, 123.2, 114.4, 112.9, 108.6, 98.3, 78.5, 56.8, 56.5, 54.6, 42.6, 28.7, 18.8, 17.4; MS-ESI *m/z* 468 [MH⁺]; HRMS-FD calcd for C₂₄H₂₉N₅O₅ (M⁺) *m/z* = 467.21632; found, 467.21623; mp 143.9 °C.

***tert*-Butyl (1-(7-(3,4-dimethoxyphenyl)pyrazolo[1,5-*a*]pyrimidine-2-carboxamido)piperidin-4-yl)carbamate (14c).** **4** (80 mg, 0.27 mmol), *tert*-butyl *N*-(4-piperidyl)carbamate (64 mg, 0.32 mmol), HBTU (152 mg, 0.40 mmol), and diisopropylethylamine (0.14 mL, 0.80 mmol) were combined in DCM (3 mL). After stirring for 24 h at r.t., the reaction mixture was extracted by DCM and aq NaHCO₃. The reaction mixture was purified by MPLC, elution gradient 2 to 5% MeOH in DCM, to give **14c** (124.8 mg, 97%) as a yellow solid. ¹H

NMR (400 MHz, DMSO- d_6) δ 8.65 (d, J = 4.5 Hz, 1H), 7.82 (dd, J = 8.5, 2.1 Hz, 1H), 7.76 (d, J = 2.1 Hz, 1H), 7.37 (d, J = 4.5 Hz, 1H), 7.19 (d, J = 8.5 Hz, 1H), 6.99 (s, 1H), 6.92 (d, J = 7.6 Hz, 1H), 4.44–4.24 (m, 2H), 3.88 (s, 3H), 3.85 (s, 3H), 3.65–3.48 (m, 1H), 3.30–3.20 (m, 1H), 3.04–2.92 (m, 1H), 2.91–2.83 (m, 2H), 1.88–1.69 (m, 2H), 1.39 (s, 9H); ^{13}C NMR (100 MHz, DMSO- d_6) δ 162.5, 155.3, 151.8, 151.0, 150.8, 149.9, 148.8, 146.1, 123.5, 122.7, 113.3, 111.8, 108.7, 97.7, 78.1, 56.20, 56.17, 54.1, 47.6, 45.8, 42.3, 41.2, 33.1, 32.0, 28.7, 18.5, 17.2, 13.0; MS-ESI m/z 504 [MNa $^+$]; HRMS-FD calcd for C₂₃H₃₁N₅O₅ (M $^+$) m/z = 481.23197; found, 481.23171; mp 162.7 °C; HPLC purity: 98.97%.

tert-Butyl 4-(7-(3,4-dimethoxyphenyl)pyrazolo[1,5-*a*]pyrimidine-2-carbonyl)piperazine-1-carboxylate (14d). **4** (300 mg, 1.00 mmol), *tert*-butyl piperazine-1-carboxylate (224 mg, 1.20 mmol), HBTU (570 mg, 1.50 mmol), and diisopropylethylamine (0.52 mL, 3.01 mmol) were combined in DCM (10 mL). After stirring for 24 h at r.t., the reaction mixture was extracted by DCM and aq NaHCO₃. The reaction mixture was purified by MPLC, elution gradient 2 to 5% MeOH in DCM, to give **14d** (384 mg, 82%) as a yellow solid. ^1H NMR (400 MHz, DMSO- d_6) δ 8.66 (d, J = 4.4 Hz, 1H), 7.83 (dd, J = 8.5, 2.0 Hz, 1H), 7.77 (d, J = 2.0 Hz, 1H), 7.39 (d, J = 4.5 Hz, 1H), 7.21 (d, J = 8.6 Hz, 1H), 7.04 (s, 1H), 3.93–3.78 (m, 8H), 3.73–3.61 (m, 2H), 3.50–3.41 (m, 2H), 3.39–3.34 (m, 2H), 1.42 (s, 9H); ^{13}C NMR (100 MHz, DMSO- d_6) δ 162.7, 154.3, 151.8, 150.9, 150.5, 149.9, 148.8, 146.2, 123.6, 122.7, 113.3, 111.9, 108.8, 98.1, 79.7, 56.20, 56.18, 46.8, 42.2, 28.5; MS-ESI m/z 468 [MH $^+$]; HRMS-FD calcd for C₂₄H₂₉N₅O₅ (M $^+$) m/z = 467.21632; found, 467.21648; mp 70.8 °C; HPLC purity: 98.72%.

tert-Butyl 4-(7-(3,4-dimethoxyphenyl)pyrazolo[1,5-*a*]pyrimidine-2-carbonyl)-2,2-dimethylpiperazine-1-carboxylate (14e). **4** (150 mg, 0.50 mmol), *tert*-butyl 2,2-dimethylpiperazine-1-carboxylate (129 mg, 0.60 mmol), HBTU (285 mg, 0.75 mmol), and diisopropylethylamine (0.26 mL, 1.50 mmol) were combined in DCM (5 mL). After stirring for 24 h at r.t., the reaction mixture was extracted by DCM and aq NaHCO₃. The reaction mixture was purified by MPLC, elution gradient 50 to 65% EA in hexane, to give **14e** (218 mg, 88%) as a yellow solid. ^1H NMR (400 MHz, DMSO- d_6) δ 8.66 (d, J = 4.4 Hz, 1H), 7.95–7.66 (m, 2H), 7.38 (dd, J = 10.5, 4.4 Hz, 1H), 7.19 (dd, J = 11.7, 8.5 Hz, 1H), 7.07 (d, J = 28.1 Hz, 1H), 4.04–3.91 (m, 2H), 3.91–3.80 (m, 6H), 3.78–3.52 (m, 4H), 1.51–1.35 (m, 12H), 1.26 (s, 3H); MS-ESI m/z 496 [MH $^+$].

tert-Butyl (S)-4-(7-(3,4-dimethoxyphenyl)pyrazolo[1,5-*a*]pyrimidine-2-carbonyl)-2-methylpiperazine-1-carboxylate (14f). **4** (250 mg, 0.84 mmol), *tert*-butyl (2S)-2-methylpiperazine-1-carboxylate (201 mg, 1.00 mmol), HBTU (475 mg, 1.25 mmol), and diisopropylethylamine (0.29 mL, 1.67 mmol) were combined in DCM (8 mL). After stirring for 24 h at r.t., the reaction mixture was extracted by DCM and aq NaHCO₃. The reaction mixture was purified by MPLC, elution gradient 50 to 65% EA in hexane, to give **14f** (180 mg, 45%) as a yellow solid. ^1H NMR (400 MHz, DMSO- d_6) δ 8.66 (d, J = 4.4 Hz, 1H), 7.87–7.64 (m, 2H), 7.39 (dd, J = 7.8, 4.5 Hz, 1H), 7.20 (dd, J = 8.4, 4.8 Hz, 1H), 7.05 (d, J = 21.4 Hz, 1H), 4.51–4.02 (m, 3H), 3.93–3.63 (m, 7H), 3.26–2.86 (m, 3H), 1.41 (d, J = 2.2 Hz, 9H), 1.05 (dd, J = 33.4, 6.7 Hz, 3H); MS-ESI m/z 482 [MH $^+$].

tert-Butyl (R)-4-(7-(3,4-dimethoxyphenyl)pyrazolo[1,5-*a*]pyrimidine-2-carbonyl)-2-methylpiperazine-1-carboxylate (14g). **4** (150 mg, 0.50 mmol), *tert*-butyl (2R)-2-methylpiperazine-1-carboxylate (120 mg, 0.60 mmol), HBTU (285 mg, 0.75 mmol), and diisopropylethylamine (0.26 mL, 1.50 mmol) were combined in DCM (5 mL). After stirring for 24 h at r.t., the reaction mixture was extracted by DCM and aq NaHCO₃. The reaction mixture was purified by MPLC, elution gradient 50 to 65% EA in hexane, to give **14g** (248 mg, >99%) as a yellow solid. ^1H NMR (400 MHz, CDCl₃) δ 8.59–8.53 (m, 1H), 7.74–7.58 (m, 2H), 7.15 (d, J = 7.5 Hz, 1H), 7.07–6.95 (m, 2H), 4.70–4.18 (m, 3H), 4.03–3.80 (m, 7H), 3.43–2.87 (m, 3H), 1.51–1.41 (m, 9H), 1.24–1.08 (m, 3H); MS-ESI m/z 482 [MH $^+$].

(7-(3,4-Dimethoxyphenyl)pyrazolo[1,5-*a*]pyrimidin-2-yl)(4-phenylpiperazin-1-yl)methanone (14h). **4** (80 mg, 0.27 mmol), 1-phenylpiperazine (52 mg, 0.32 mmol), HBTU (152 mg, 0.40 mmol), and diisopropylethylamine (0.14 mL, 0.80 mmol) were combined in DCM (3 mL). After stirring for 24 h at r.t., the reaction mixture was

extracted by DCM and aq NaHCO₃. The reaction mixture was purified by MPLC, elution gradient 50 to 75% EA in hexane, to give **14h** (135.1 mg, >99%) as a yellow solid. ^1H NMR (400 MHz, DMSO- d_6) δ 8.67 (d, J = 4.4 Hz, 1H), 7.85 (dd, J = 8.5, 2.1 Hz, 1H), 7.80 (d, J = 2.1 Hz, 1H), 7.41 (d, J = 4.5 Hz, 1H), 7.31–7.15 (m, 3H), 7.07 (s, 1H), 6.97 (d, J = 7.9 Hz, 2H), 6.82 (t, J = 7.3 Hz, 1H), 4.05–3.92 (m, 2H), 3.91–3.78 (m, 8H), 3.28–3.21 (m, 2H), 3.21–3.11 (m, 2H); ^{13}C NMR (100 MHz, DMSO- d_6) δ 162.5, 151.8, 151.2, 150.9, 150.7, 149.9, 148.8, 146.1, 129.5, 123.6, 122.7, 119.9, 116.3, 113.3, 111.9, 108.8, 98.1, 56.23, 56.19, 49.5, 48.9, 46.9, 42.3; MS-ESI m/z 444 [MH $^+$]; HRMS-FD calcd for C₂₅H₂₅N₅O₃ (M $^+$) m/z = 443.19519; found, 443.19590; mp 118.4 °C.

(7-(3,4-Dimethoxyphenyl)pyrazolo[1,5-*a*]pyrimidin-2-yl)(4-methylpiperazin-1-yl)methanone (14i). **4** (50 mg, 0.17 mmol), 1-methylpiperazine (0.023 mL, 0.20 mmol), HBTU (95.0 mg, 0.25 mmol), and diisopropylethylamine (0.09 mL, 0.50 mmol) were combined in DCM (2 mL). After stirring for 24 h at r.t., the reaction mixture was extracted by DCM and aq NaHCO₃. The reaction mixture was purified by MPLC, elution gradient 2 to 5% MeOH in DCM, to give **14i** (52.8 mg, 83%) as a pale-yellow solid. ^1H NMR (400 MHz, DMSO- d_6) δ 8.65 (d, J = 4.5 Hz, 1H), 7.85–7.74 (m, 2H), 7.38 (d, J = 4.4 Hz, 1H), 7.20 (d, J = 8.2 Hz, 1H), 7.01 (s, 1H), 3.88 (s, 3H), 3.86 (s, 3H), 3.83–3.77 (m, 2H), 3.72–3.61 (m, 2H), 2.43–2.35 (m, 2H), 2.35–2.28 (m, 2H), 2.21 (s, 3H); ^{13}C NMR (100 MHz, DMSO- d_6) δ 162.5, 151.8, 150.84, 150.76, 149.9, 148.7, 146.1, 123.5, 122.7, 113.2, 111.8, 108.7, 97.9, 56.2, 56.1, 55.5, 54.8, 46.9, 46.0, 42.2; MS-ESI m/z 382 [MH $^+$]; HRMS-FD calcd for C₂₀H₂₃N₅O₃ (M $^+$) m/z = 381.17954; found, 381.17925; mp 150.6 °C; HPLC purity: 98.54%.

(7-(3,4-Dimethoxyphenyl)pyrazolo[1,5-*a*]pyrimidin-2-yl)(4-isopropylpiperazin-1-yl)methanone (14j). **4** (50 mg, 0.17 mmol), 1-isopropylpiperazine (0.029 mL, 0.20 mmol), HBTU (95.0 mg, 0.25 mmol), and diisopropylethylamine (0.09 mL, 0.50 mmol) were combined in DCM (2 mL). After stirring for 24 h at r.t., the reaction mixture was extracted by DCM and aq NaHCO₃. The reaction mixture was purified by MPLC, elution gradient 2 to 5% MeOH in DCM, to give **14j** (58.6 mg, 86%) as a yellow solid. ^1H NMR (400 MHz, DMSO- d_6) δ 8.65 (d, J = 4.5 Hz, 1H), 7.86–7.72 (m, 2H), 7.38 (d, J = 4.5 Hz, 1H), 7.20 (d, J = 8.4 Hz, 1H), 7.00 (s, 1H), 3.88 (s, 3H), 3.85 (s, 3H), 3.81–3.71 (m, 2H), 3.71–3.59 (m, 2H), 2.77–2.60 (m, 1H), 2.46–2.39 (m, 2H), 0.97 (d, J = 6.5 Hz, 6H); ^{13}C NMR (100 MHz, DMSO- d_6) δ 162.4, 151.8, 150.9, 150.7, 149.9, 148.7, 146.1, 123.6, 122.7, 113.3, 111.8, 108.7, 97.9, 56.17, 56.15, 55.4, 49.0, 48.2, 18.3; MS-ESI m/z 410 [MH $^+$]; HRMS-FD calcd for C₂₂H₂₇N₅O₃ (M $^+$) m/z = 409.21084; found, 409.21099; mp 155.9 °C; HPLC purity: 98.12%.

(4-Cyclopropylpiperazin-1-yl)(7-(3,4-dimethoxyphenyl)pyrazolo[1,5-*a*]pyrimidin-2-yl)methanone (14k). **4** (50 mg, 0.17 mmol), 1-cyclopropylpiperazine (0.027 mL, 0.20 mmol), HBTU (95.0 mg, 0.25 mmol), and diisopropylethylamine (0.09 mL, 0.50 mmol) were combined in DCM (2 mL). After stirring for 24 h at r.t., the reaction mixture was extracted by DCM and aq NaHCO₃. The reaction mixture was purified by MPLC, elution gradient 2 to 5% MeOH in DCM, to give **14k** (58.2 mg, 85%) as a pale-yellow solid. ^1H NMR (400 MHz, DMSO- d_6) δ 8.65 (d, J = 4.5 Hz, 1H), 7.84–7.74 (m, 2H), 7.38 (d, J = 4.5 Hz, 1H), 7.20 (d, J = 8.4 Hz, 1H), 7.01 (s, 1H), 3.88 (s, 3H), 3.85 (s, 3H), 3.78–3.70 (m, 2H), 3.69–3.58 (m, 2H), 2.65–2.57 (m, 2H), 2.55–2.52 (m, 2H), 1.71–1.57 (m, 1H), 0.48–0.40 (m, 2H), 0.37–0.28 (m, 2H); ^{13}C NMR (100 MHz, DMSO- d_6) δ 162.5, 151.8, 150.9, 150.8, 149.9, 148.7, 146.1, 123.5, 122.7, 113.2, 111.8, 108.7, 97.9, 56.18, 56.15, 53.7, 53.0, 47.0, 42.2, 38.4, 6.2; MS-ESI m/z 408 [MH $^+$]; HRMS-FD calcd for C₂₂H₂₅N₅O₃ (M $^+$) m/z = 407.19519; found, 407.19567; mp 139.5 °C; HPLC purity: 98.60%.

(4-(Cyclopropanecarbonyl)piperazin-1-yl)(7-(3,4-dimethoxyphenyl)pyrazolo[1,5-*a*]pyrimidin-2-yl)methanone (14l). **4** (50 mg, 0.17 mmol), cyclopropylpiperazin-1-yl)methanone hydrochloride (38.2 mg, 0.20 mmol), HBTU (95.0 mg, 0.25 mmol), and diisopropylethylamine (0.09 mL, 0.50 mmol) were combined in DCM (2 mL). After stirring for 24 h at r.t., the reaction mixture was extracted by DCM and aq NaHCO₃. The reaction mixture was purified by MPLC, elution gradient 2 to 5% MeOH in DCM. The crude mixture was solidified using DCM and hexane to give **14l** (48.3 mg, 66%) as a

pale-yellow solid. $^1\text{H NMR}$ (400 MHz, DMSO- d_6) δ 8.67 (d, J = 4.5 Hz, 1H), 7.92–7.80 (m, 1H), 7.77 (s, 1H), 7.43–7.35 (m, 1H), 7.21 (d, J = 8.4 Hz, 1H), 7.06 (s, 1H), 3.98–3.44 (m, 14H), 2.12–1.89 (m, 1H), 0.85–0.59 (m, 4H); $^{13}\text{C NMR}$ (100 MHz, DMSO- d_6) δ 171.8, 162.7, 151.8, 150.9, 150.5, 149.9, 148.8, 146.2, 123.6, 122.6, 113.2, 111.8, 108.8, 98.2, 56.2, 47.2, 46.9, 45.8, 45.0, 42.7, 42.5, 42.3, 41.7, 10.8, 7.6; MS-ESI m/z 436 [MH^+]; HRMS-FD calcd for $\text{C}_{23}\text{H}_{25}\text{N}_5\text{O}_4$ (M^+) m/z = 435.19011; found, 435.19080; mp 67.7 °C; HPLC purity: 98.83%.

(7-(3,4-Dimethoxyphenyl)pyrazolo[1,5-*a*]pyrimidin-2-yl)-(piperazin-1-yl)methanone (15a). 14d (50 mg, 0.107 mmol) was dissolved in MeOH (1 mL), followed by addition of hydrogen chloride in dioxane (4 N, 0.27 mL) and stirring at r.t. for 26 h. The crude mixture was solidified using diethyl ether to give 15a (25.5 mg, 59%) as an orange solid. $^1\text{H NMR}$ (400 MHz, DMSO- d_6) δ 9.25 (s, 2H), 8.68 (d, J = 4.4 Hz, 1H), 7.81 (d, J = 8.5 Hz, 1H), 7.76 (s, 1H), 7.41 (d, J = 4.4 Hz, 1H), 7.20 (d, J = 8.6 Hz, 1H), 7.10 (s, 1H), 4.23–4.03 (m, 2H), 3.98–3.76 (m, 8H), 3.36–3.09 (m, 4H); $^{13}\text{C NMR}$ (100 MHz, DMSO- d_6) δ 162.6, 151.8, 151.1, 149.9, 148.8, 146.2, 123.5, 122.6, 113.2, 111.8, 109.0, 98.5, 56.25, 56.19, 44.0, 43.4, 42.9, 39.2; MS-ESI m/z 368 [MH^+]; HRMS-FD calcd for $\text{C}_{16}\text{H}_{21}\text{N}_5\text{O}_3$ (M^+) m/z = 367.16389; found, 367.16368; mp 94.8 °C; HPLC purity: 98.54%.

(7-(3,4-Dimethoxyphenyl)pyrazolo[1,5-*a*]pyrimidin-2-yl)-(3,3-dimethylpiperazin-1-yl)methanone (15b). 14e (218 mg, 0.44 mmol) and TFA (0.34 mL, 4.40 mmol) were combined in DCM (1 mL) at r.t. for 4 h. After evaporation, the reaction mixture was extracted by DCM and aq NaHCO_3 . The organic layer was dried over anhydrous MgSO_4 and concentrated in vacuo to give 15b (129.7 mg, 75%) as a yellow solid. $^1\text{H NMR}$ (400 MHz, DMSO- d_6) δ 8.64 (dd, J = 4.4, 2.0 Hz, 1H), 7.85–7.70 (m, 2H), 7.37 (dd, J = 11.6, 4.5 Hz, 1H), 7.18 (t, J = 8.4 Hz, 1H), 6.98 (d, J = 20.0 Hz, 1H), 3.90–3.83 (m, 6H), 3.68–3.59 (m, 1H), 3.59–3.52 (m, 1H), 3.51 (s, 1H), 3.40 (s, 1H), 2.85–2.70 (m, 2H), 1.06 (s, 3H), 0.93 (s, 3H); MS-ESI m/z 396 [MH^+].

(5)-(7-(3,4-Dimethoxyphenyl)pyrazolo[1,5-*a*]pyrimidin-2-yl)(3-methylpiperazin-1-yl)methanone (15c). 14f (22 mg, 0.046 mmol) and TFA (0.034 mL, 0.46 mmol) were combined in DCM (0.5 mL) at r.t. for 4 h. After evaporation, the reaction mixture was extracted by DCM and aq NaHCO_3 . The organic layer was dried over anhydrous MgSO_4 and concentrated in vacuo to give 15c (10.6 mg, 61%) as a yellow solid. $^1\text{H NMR}$ (400 MHz, DMSO- d_6) δ 8.65 (d, J = 4.4 Hz, 1H), 7.87–7.69 (m, 2H), 7.44–7.32 (m, 1H), 7.18 (t, J = 8.3 Hz, 1H), 6.99 (s, 1H), 4.43–4.18 (m, 2H), 3.87 (s, 3H), 3.85 (s, 3H), 3.15–2.90 (m, 1H), 2.87–2.56 (m, 4H), 2.47–2.36 (m, 1H), 1.05–0.80 (m, 3H); MS-ESI m/z 382 [MH^+].

(R)-(7-(3,4-Dimethoxyphenyl)pyrazolo[1,5-*a*]pyrimidin-2-yl)(3-methylpiperazin-1-yl)methanone (15d). 14g (241 mg, 0.50 mmol) and TFA (0.38 mL, 5.01 mmol) were combined in DCM (5 mL) at r.t. for 4 h. After evaporation, the reaction mixture was extracted by DCM and aq NaHCO_3 . The organic layer was dried over anhydrous MgSO_4 and concentrated in vacuo to give 15d (129.4 mg, 68%) as a yellow solid. $^1\text{H NMR}$ (400 MHz, CDCl_3) δ 8.60–8.52 (m, 1H), 7.76–7.65 (m, 2H), 7.12–7.07 (m, 1H), 7.06–6.95 (m, 2H), 4.71–4.43 (m, 2H), 4.01–3.87 (m, 6H), 3.26–3.07 (m, 1H), 3.01–2.45 (m, 4H), 1.18–0.95 (m, 3H); MS-ESI m/z 382 [MH^+].

(4-Benzylpiperazin-1-yl)(7-(3,4-dimethoxyphenyl)pyrazolo[1,5-*a*]pyrimidin-2-yl)methanone (16a). 15a (75 mg, 0.19 mmol), benzyl bromide (0.066 mL, 0.56 mmol), and potassium carbonate (128 mg, 0.93 mmol) were combined in DMF (1 mL). After stirring for 3 h at r.t., the reaction mixture was extracted by DCM and aq NaCl . The reaction mixture was purified by MPLC, elution gradient 60 to 80% EA in hexane, to give 16a (50.2 mg, 59%) as a yellow solid. $^1\text{H NMR}$ (400 MHz, DMSO- d_6) δ 8.65 (d, J = 4.5 Hz, 1H), 7.85–7.72 (m, 2H), 7.42–7.30 (m, 5H), 7.30–7.24 (m, 1H), 7.19 (d, J = 8.6 Hz, 1H), 7.01 (s, 1H), 3.88 (s, 3H), 3.86–3.75 (m, 5H), 3.74–3.64 (m, 2H), 3.52 (s, 2H), 2.47–2.42 (m, 2H), 2.42–2.36 (m, 2H); $^{13}\text{C NMR}$ (100 MHz, DMSO- d_6) δ 162.5, 151.8, 150.82, 150.75, 149.9, 148.7, 146.1, 138.2, 129.4, 129.4, 128.7, 128.7, 127.5, 123.5, 122.7, 113.3, 111.8, 108.7, 97.9, 62.3, 56.2, 56.2, 53.5, 52.7, 47.1, 42.3; MS-ESI m/z 458 [MH^+]; HRMS-FD calcd for $\text{C}_{26}\text{H}_{27}\text{N}_5\text{O}_3$ (M^+) m/z = 457.21084; found, 457.21046; mp 62.0 °C; HPLC purity: 96.82%.

(4-Benzoylpiperazin-1-yl)(7-(3,4-dimethoxyphenyl)pyrazolo[1,5-*a*]pyrimidin-2-yl)methanone (16b). 15a (75 mg, 0.19 mmol), benzoyl chloride (0.03 mL, 0.28 mmol), and diisopropylethylamine (0.16 mL, 0.93 mmol) were combined in DCM (2 mL). After stirring for 24 h at r.t., the reaction mixture was extracted by DCM and aq NaCl . The reaction mixture was purified by MPLC, elution gradient 5 to 9% MeOH in DCM, to give 16b (50.3 mg, 67%) as a yellow solid. $^1\text{H NMR}$ (400 MHz, DMSO- d_6) δ 8.66 (d, J = 4.1 Hz, 1H), 8.01–7.66 (m, 2H), 7.54–7.31 (m, 6H), 7.28–7.09 (m, 1H), 7.05 (s, 1H), 4.03–3.56 (m, 12H), 3.56–3.40 (m, 2H); $^{13}\text{C NMR}$ (100 MHz, DMSO- d_6) δ 169.7, 162.7, 151.8, 150.9, 150.5, 149.9, 148.8, 146.2, 136.1, 130.1, 128.9, 127.5, 123.6, 122.7, 113.3, 111.9, 108.9, 98.2, 56.2, 56.2, 47.1, 42.4; MS-ESI m/z 472 [MH^+]; HRMS-FD calcd for $\text{C}_{26}\text{H}_{25}\text{N}_5\text{O}_4$ (M^+) m/z = 471.19011; found, 471.19034; mp 88.6 °C; HPLC purity: 97.51%.

(4-Benzoyl-3,3-dimethylpiperazin-1-yl)(7-(3,4-dimethoxyphenyl)pyrazolo[1,5-*a*]pyrimidin-2-yl)methanone (16c). 15b (120 mg, 0.30 mmol), benzoyl chloride (0.05 mL, 0.46 mmol), and triethylamine (0.21 mL, 1.52 mmol) were combined in DCM (3 mL). After stirring for 24 h at r.t., the reaction mixture was extracted by DCM and aq NaHCO_3 . The reaction mixture was purified by MPLC, elution gradient 5 to 9% MeOH in DCM. The crude mixture was solidified using EA and hexane to give 16c (126.2 mg, 83%) as a pale-yellow solid. $^1\text{H NMR}$ (400 MHz, DMSO- d_6) δ 8.70–8.60 (m, 1H), 7.88–7.67 (m, 2H), 7.51–7.31 (m, 6H), 7.24–7.00 (m, 2H), 4.14–3.77 (m, 8H), 3.71–3.48 (m, 4H), 1.64–1.35 (m, 6H); $^{13}\text{C NMR}$ (100 MHz, DMSO- d_6) δ 171.2, 163.5, 152.5, 150.9, 150.8, 150.1, 149.4, 146.3, 138.6, 129.7, 128.8, 126.9, 123.7, 123.3, 114.7, 112.9, 108.8, 99.4, 57.8, 56.8, 56.6, 23.9; MS-ESI m/z 500 [MH^+]; HRMS-FD calcd for $\text{C}_{28}\text{H}_{29}\text{N}_5\text{O}_4$ (M^+) m/z = 499.22141; found, 499.22111; mp 87.7 °C; HPLC purity: 97.26%.

(S)-(4-Benzoyl-3-methylpiperazin-1-yl)(7-(3,4-dimethoxyphenyl)pyrazolo[1,5-*a*]pyrimidin-2-yl)methanone (16d). 15c (3258 mg, 8.54 mmol), benzoyl chloride (1.48 mL, 12.8 mmol), and triethylamine (5.95 mL, 42.7 mmol) were combined in DCM (85 mL). After stirring for 24 h at r.t., the reaction mixture was extracted by DCM and aq NaHCO_3 . The reaction mixture was purified by MPLC, elution gradient 5 to 9% MeOH in DCM. The crude mixture was solidified using EA and hexane to give 16d (2509 mg, 61%) as a pale-yellow solid. $^1\text{H NMR}$ (400 MHz, CDCl_3) δ 8.59–8.54 (m, 1H), 7.75–7.55 (m, 2H), 7.49–7.34 (m, 5H), 7.17 (d, J = 7.4 Hz, 1H), 7.07–6.96 (m, 2H), 4.98–4.47 (m, 3H), 4.05–3.79 (m, 7H), 3.54–2.83 (m, 3H), 1.38–1.14 (m, 3H); $^{13}\text{C NMR}$ (100 MHz, DMSO- d_6) δ 169.1, 162.6, 151.6, 149.8, 149.7, 149.2, 148.4, 145.3, 135.9, 128.8, 127.9, 126.1, 122.8, 122.2, 113.7, 111.8, 107.7, 97.4, 55.8, 55.6, 47.3, 14.8; MS-ESI m/z 486 [MH^+]; HRMS-FD calcd for $\text{C}_{27}\text{H}_{27}\text{N}_5\text{O}_4$ (M^+) m/z = 485.20576; found, 485.20555; mp 83.5 °C; HPLC purity: 99.97%.

(R)-(4-Benzoyl-3-methylpiperazin-1-yl)(7-(3,4-dimethoxyphenyl)pyrazolo[1,5-*a*]pyrimidin-2-yl)methanone (16e). 15d (120 mg, 0.30 mmol), benzoyl chloride (0.05 mL, 0.46 mmol), and triethylamine (0.21 mL, 1.52 mmol) were combined in DCM (3 mL). After stirring for 24 h at r.t., the reaction mixture was extracted by DCM and aq NaHCO_3 . The reaction mixture was purified by MPLC, elution gradient 5 to 9% MeOH in DCM. The crude mixture was solidified using EA and hexane to give 16e (127.4 mg, 83%) as a pale-yellow solid. $^1\text{H NMR}$ (400 MHz, CDCl_3) δ 8.57 (s, 1H), 7.75–7.54 (m, 2H), 7.49–7.33 (m, 5H), 7.17 (d, J = 7.4 Hz, 1H), 7.07–6.94 (m, 2H), 5.04–4.44 (m, 3H), 4.07–3.85 (m, 7H), 3.51–2.85 (m, 3H), 1.37–1.22 (m, 3H); $^{13}\text{C NMR}$ (100 MHz, DMSO- d_6) δ 169.1, 162.6, 151.5, 149.8, 149.7, 149.2, 148.4, 145.3, 135.9, 128.8, 127.9, 126.0, 122.8, 122.2, 113.7, 111.8, 107.7, 97.3, 55.8, 55.6, 47.2, 14.8; MS-ESI m/z 486 [MH^+]; HRMS-FD calcd for $\text{C}_{27}\text{H}_{27}\text{N}_5\text{O}_4$ (M^+) m/z = 485.20576; found, 485.20595; mp 94.8 °C; HPLC purity: 98.28%.

YFP Fluorescence Quenching Assay. CHO-K1 cells expressing wild-type human CFTR with the halide sensor YFP-H148Q/I152L were plated in 96-well microplates at a density of 2×10^4 cells per well. CHO-CFTR-YFP cells were incubated for 48 h at 37 °C. Assays were done using FLUOstar Omega microplate reader (BMG labtech, Allmendgrün, Ortenberg, Germany) and MARS Data Analysis

Software (BMG labtech). Briefly, each well of a 96-well plate was washed three times in PBS (200 μL /wash). Then, 100 μL of PBS was added to each well. Test compounds (1 μL) were added to each well at a final concentration of 25 μM . After 10 min, 96-well plates were transferred to the microplate reader preheated to 37 $^{\circ}\text{C}$ for fluorescence assay. Each well was assayed individually for CFTR-mediated I^{-} influx by recording fluorescence continuously (400 ms per point) for 2 s (baseline). Then, 100 μL of 140 mM I^{-} solution was added at 2 s, and then YFP fluorescence was recorded for 14 s. Initial iodide influx rate was determined from the initial slope of fluorescence decrease, by nonlinear regression, following infusion of iodide.

Solubility Test Protocol. PBS (pH 7.5) was prepared by mixing 81% 0.0667 M Na_2HPO_4 and 19% 0.0667 M NaH_2PO_4 , and NaCl was added to adjust isotonicity. Then, test compounds were dissolved in PBS (pH 7.5) at 0.5 mg/mL and vortexed for 90 min, after which the compound solutions dissolved in PBS were sequentially filtered through a 0.45, 1.2, 5.0 μm syringe filter (Minisart NML, CA). The concentration of filtered test compounds was measured by LC-MS/MS using an Agilent 1290 Infinity UPLC coupled with Sciex Triple Quadrupole 5500 system with the appropriate dilution of the samples. To quantify the concentration of test compounds, all calibration curves consisted of at least six calibrator concentrations, a blank sample (with internal standard), and a double blank sample (without internal standard). The calibration curves were constructed by the weighted linear or quadratic regression method ($1/x$) of peak area ratios of analyte to internal standard versus actual concentration. The solubility of the test compounds was back-calculated by substituting peak area ratios of analyte to internal standard of filtered test compounds into the calibration curve.

Molecular Docking Simulation. All applications in the molecular docking simulation were provided in Maestro module of Schrödinger Suite 2022-2.³⁰ The cryo-EM structure of CFTR was obtained from protein data bank (PDB id: 6O2P),²⁵ which was prepared with Protein Preparation Wizard. The receptor grid was generated 20 \times 20 \times 20 \AA space region centered at the co-ligand of the complex structure, and then the low-energy 3D structures of Cact-3, **16d**, and **16e** were docked with default values in SP mode using Glide module. Using the structure of protein–ligand complex corresponding to the best pose of Cact-3, **16d**, and **16e**, the protein residues that have atoms within 3 \AA of the ligand were refined in the environment with an implicit membrane by Refine Protein–Ligand Complex module. We calculated each binding energy of **16d**/**16e** using the MM-GBSA method with Prime, where the implicit membrane was also considered. The protein–ligand interactions were analyzed by Discovery Studio Modeling Environment v4.026 (BIOVIA, San Diego, CA, USA), and the docking models were displayed using PyMOL version 2.0.47.

Ussing Chamber Experiment. Snapwell (Corning Inc., NY, USA) inserts containing CFTR-expressing FRT cells and primary cultured human conjunctival epithelial cells were mounted in Ussing chambers. For the measurement of apical membrane current in FRT-CFTR cells, the apical bath was filled with a half- Cl^{-} solution and the basolateral bath was filled with HCO_3^{-} -buffered solution to generate transepithelial Cl^{-} gradient (apical, 64 mM; basolateral, 129 mM), and the basolateral membrane was permeabilized with 250 $\mu\text{g}/\text{mL}$ amphotericin B. For short-circuit current measurements in primary cultured human conjunctival epithelial cells, apical and basolateral baths were filled with HCO_3^{-} -buffered solution. Cells were bathed for a 20 min stabilization period and aerated with 95% O_2 /5% CO_2 at 37 $^{\circ}\text{C}$. Forskolin, **16d**, and CFTR_{inh}-172 were added to the apical and basolateral bath solutions. Apical membrane current and short-circuit current were measured with an EVC4000 Multi-Channel V/I Clamp (World Precision Instruments, Sarasota, FL) and recorded using PowerLab 4/35 (AD Instruments, Colorado Springs, CO, USA). Data were collected and analyzed with Labchart Pro 7 software (AD Instruments). The sampling rate was 4 Hz.

Pharmacokinetics and Ocular Tissue Distribution Study. The purpose of this study was to determine the plasma pharmacokinetics and ocular tissue distribution of **16d** following topical instillation at a volume of 50 $\mu\text{L}/\text{eye}$ (0.1 mg/eye) to the right eye of naive male New Zealand White Rabbit. **16d** was monitored in plasma and ocular tissues

(from one eye) for up to 72 h **16d** used in this experiment was dissolved in 5% Polyoxyl 35 castor oil in sodium phosphate buffer. Animals were administered **16d** Eye Drops by single topical instillation administration at 0.1 mg/eye. Plasma, tear, cornea, conjunctiva, and retina samples were collected at 0.5, 1, 4, 8, 12, 24, 48, and 72 h post-dose. Concentrations of **16d** in plasma, tear, cornea homogenate, conjunctiva homogenate, and retina homogenate samples were determined by a liquid chromatography–tandem mass spectrometry (LC-MS/MS) method. The plasma, tear, cornea, conjunctiva, and retina concentration of **16d** in study animals was subjected to a non-compartmental pharmacokinetic analysis by using the Phoenix WinNonlin software (version 6.3 or above, Pharsight). The linear/log trapezoidal rule was applied in obtaining the PK parameters. Tear, cornea, conjunctiva, retina, aqueous humor, and lacrimal gland concentration values that were below the lower limit of quantitation (LLOQ) were excluded from the PK parameter calculation.

Corneal and Conjunctival Epithelial Cytotoxicity Test. Immortalized human corneal epithelial cells and conjunctival epithelial cells (Innoprot, Bizkaia, Spain) were plated on 96-well microplates. After 24 h incubation, cells were treated with 30 μM candidate compounds or 0.01% Triton X-100 (Sigma-Aldrich, St Louis, MO, USA), and then they were incubated for 2 days. An equal amount of DMSO was added to the control. The culture medium and the compounds were changed every 12 h. To assess cell proliferation after 48 h of incubation with the compound, the cells were re-incubated with MTS for 1 h. The soluble formazan produced by cellular reduction of MTS was quantified by measuring the absorbance at 490 nm with infinite M200 microplate reader (Infinite M200 Pro, Tecan Group Ltd., Grödig, Austria). MTS assay was done using CellTiter 96 Aqueous One Solution Cell Proliferation Assay kit (Promega, Madison, WI, USA).

Whole-Cell Patch Clamp. Whole-cell, patch-clamp recordings were performed on CFTR-expressing CHO-K1 cells. The bath solution contained (in mM) 140 NMDG-Cl, 1 CaCl_2 , 1 MgCl_2 , 10 glucose, and 10 HEPES (pH 7.4). The pipette solution contained (in mM) 130 CsCl, 0.5 EGTA, 1 MgCl_2 , 1 Tris-ATP, and 10 HEPES (pH 7.2). Pipettes were pulled from borosilicate glass and had resistances of 3–5 $\text{M}\Omega$ after fire polishing. Seal resistances were between 3 and 10 $\text{G}\Omega$. After establishing the whole-cell configuration, CFTR was activated by forskolin and/or **16d**. Whole-cell currents were elicited by applying hyperpolarizing and depolarizing voltage pulses from a holding potential of 0 mV to potentials between -80 and $+80$ mV in steps of 20 mV. Recordings were made at room temperature using an Axopatch-200B (Axon instruments, Foster City, CA, USA). Currents were digitized with a Digidata 1440A converter (Molecular Devices Co., Union City, CA USA), filtered at 5 kHz, and sampled at 1 kHz.

ANO1 Activity Measurement. Snapwell inserts containing FRT cells expressing human ANO1 were mounted in Ussing chambers. The apical bath was filled with a half- Cl^{-} solution, and the basolateral bath was filled with HCO_3^{-} -buffered solution to generate transepithelial Cl^{-} gradient (apical, 64 mM; basolateral, 129 mM), and the basolateral membrane was permeabilized with 250 $\mu\text{g}/\text{mL}$ amphotericin B. Cells were bathed for a 20 min stabilization period and aerated with 95% O_2 /5% CO_2 at 37 $^{\circ}\text{C}$. ATP was applied to the apical bath solution to induce intracellular calcium increase. **16d** or Ani9 was added to the apical and basolateral bath solution. 20 min before ANO1 activation, apical membrane currents were measured with an EVC4000 Multi-Channel V/I Clamp and PowerLab 4/35. Data were analyzed using Labchart Pro 7. The sampling rate was 4 Hz.

VRAC Activity Measurement. HeLa cells were stably transfected with YFP-F46L/H148Q/I152L, a halide sensor YFP. After the cells were incubated on 96-well microplates for 48 h, each well of the 96-well plate was washed three times in PBS (200 $\mu\text{L}/\text{wash}$), and the wells were filled with 50 $\mu\text{L}/\text{well}$ isotonic solution (in mM): 140 NaCl, 5 KCl, 20 HEPES (310 mOsm; pH 7.4 with NaOH). In each well, VRAC expressed on the cells were stimulated with addition of 50 μL of hypotonic solutions (in mM): 5 KCl, 20 HEPES, 90 mannitol (120 mOsm/kg). Test compounds (1 μL) were added to each well in a dose-dependent manner. After 5 min, 96-well plates were transferred to a plate reader for fluorescence assay. Each well was assayed individually for VRAC-mediated I^{-} influx by recording fluorescence continuously

(400 ms per point) for 7.6 s. YFP fluorescence was recorded 0.4 s for baseline; then 100 μL of 140 mM I^- solution was added at 0.4 s to see the change in fluorescence. Initial iodide influx rate was determined from the initial slope of fluorescence decrease, by nonlinear regression, following infusion of iodide.

Intracellular cAMP Measurement. CHO-K1 cells grown on 12-well culture plates were washed three times with PBS and then incubated in PBS containing 100 μM 3-isobutyl-1-methylxanthine (IBMX) at 37 $^{\circ}\text{C}$ for 5 min. The cells were treated with **16d** or forskolin and incubated for 10 min at 37 $^{\circ}\text{C}$. After a 10 min incubation, the cells were washed with cold PBS and cytosolic cAMP was measured using a cAMP immunoassay kit (Parameter cAMP Immunoassay Kit; R&D Systems, Minneapolis, MN) according to the manufacturer's protocol.

Animals. All animals use and care strictly conformed to the ARVO statements for the Use of Animals in Ophthalmic and Vision Research. This study was approved and reviewed by the institutional review board of Severance Hospital, Yonsei College of Medicine (Seoul, Korea) (IRB no.: 2019-0166).

Scopolamine-Induced Dry Eye Mouse Model and Application of Eyedrop. Eight weeks old female C57BL/6J mice obtained from Orientbio (Gyeonggi-do, South Korea) were used. The experimental period was carried out for a total of 24 days, and breeding is performed in a dry chamber (temperature: 22 $^{\circ}\text{C}$, humidity: 12%) during the experiment period. To induce a dry eye model, 0.5 mg/0.1 mL of scopolamine hydrobromide was injected subcutaneously three times a day (11:00 am, 2:00 pm, 5:00 pm) for 14 days. After induction of dry eye mice model, each eye drops 0.3% diquafosol sodium (Diquas, ophthalmic solution Santen Pharmaceutical Co., Ltd., Osaka, Japan), the vehicle (5% Polyoxyl 35 castor oil in sodium phosphate buffer), or **16d** (2060 μM) was applied three times a day (11:00 am, 2:00 pm, 5:00 pm) for 10 days, with simultaneous subcutaneous injection of 0.5 mg/0.1 mL of scopolamine hydrobromide for the first 8 days of treatment period. Eye drop application was done in both eyes, each 5 μL , and maintained for 30 s.

Application of Eyedrops in Wild-Type Mouse. Eight weeks old female C57BL/6J mice obtained from Orient Bio (Seongnam, South Korea) were used. After 7 days for domestication, each eye drops **16d**, and Cact-3 was applied once. Eye drop application was done in both eyes each with 2.5 μL and maintained 30 s. The experiment was conducted with different concentrations of **16d** and Cact-3. 5% Polyoxyl 35 castor oil in sodium phosphate buffer was used as a vehicle.

Tear Volume Measurement. Tear volume was measured using phenol red threads (Showa Yakuhin Kako Co., Ltd, Tokyo, Japan) by applying those in the lateral canthal areas of normal or dry eye model-treated scopolamine hydrobromide mice for 15 s using forceps, and the measurement was done using a vernier caliper to check the length of wet thread under a microscope. Measuring was implemented three times in dry eye model mice, before inducing dry eye, after inducing dry eye, and 10 days after eye drop application. In experiments with normal female C57BL/6J mice, tear volume measurement using phenol red thread was done four times, right before application of eye drop (0 h, baseline), and 1 h, 3 h, and 6 h after application of eye drops.

Corneal Erosion Grading. To evaluate corneal epithelial erosion, 5 μL of 1% fluorescein dye with 0.5% proparacaine was applied to the ocular surface of mice after 10 days of each treatment. Photographs of the ocular anterior segment were taken with the built-in digital camera in a microscope under cobalt-blue filtered light. Each corneal erosion was scored from 0 to 5 according to the Oxford scheme.³¹

Quantitative PCR Analysis. Total RNA was isolated using Tri-RNA reagent (FAVORGEN, Ping-Tung, Taiwan), and 1 μg of total RNA was used to synthesize cDNA using RNA to cDNA EcoDryTM premix (TaKaRa, Shiga, Japan) according to the manufacturer's protocol. The relative mRNA levels were evaluated in ViiA7 (Applied Biosystems, Foster City, CA, USA) using SYBR Green PCR Master Mix (Applied Biosystems). Target gene expression was normalized to that of the housekeeping gene glyceraldehyde 3-phosphate dehydrogenase (GAPDH). The primer sequences used were as follows: GAPDH, sense (5-AACGACCCCTTCATTGACCT-3) and antisense (5-ATGT-TAGTGGGGTCTCGCTC-3), size of PCR product 155 base pairs; IL-1 β , sense (5-ACTCATTGTGGCTGTGGAGA-3) and antisense

(5-TTGTTCATCTCGGAGCCTGT-3), size of PCR product 199 base pairs; IL-6, sense (5-CTGCAAGAGACTTCCATCCAG-3) and antisense (5-AGTGGTATAGACAGGTCTGTTGG-3), size of PCR product 131 base pairs; IL-17, sense (5-GCTGACCCCTAA-GAAACCCC-3) and antisense (5-GAAGCAGTTTGG-GACCCCTT-3), size of PCR product 162 base pairs; TNF- α , sense (5-AGCACAGAAAGCATGATCCG-3) and antisense (5-CGAT-CACCCCGAAGTTCAGT-3), size of PCR product 166 base pairs; MMP-2, sense (5-CGATGTCGCCCTAAAACAG-3) and antisense (5-GCATGGTCTCGATGGTGTTTC-3), size of PCR product 176 base pairs; and MMP-9, sense (5-AAAACCTCCAACCTCACGGA-3) and antisense (5-GTGGTGTTCGAATGGCCTTT-3), size of PCR product 190 base pairs.

Statistical Analysis. Student t-test was used to evaluate the significance of the differences, and $p < 0.05$ was considered as significant.

■ ASSOCIATED CONTENT

SI Supporting Information

The Supporting Information is available free of charge at <https://pubs.acs.org/doi/10.1021/acs.jmedchem.2c01382>.

Synthetic schemes; procedures; analytic data for compounds **18**, **19**, and **24a-e**; and HPLC traces for compounds **1**, **5a**, **5c-i**, **5k**, **10a-c**, **11a-c**, **12a-d**, **13a-c**, **14a**, **14c-d**, **14i-l**, **15a**, **16a-e**, **19**, **20**, and **25a-e** (PDF)
Molecular formula strings (CSV)

■ AUTHOR INFORMATION

Corresponding Authors

Hongchul Yoon – Research Laboratories, ILDONG Pharmaceutical Co., Ltd., Hwaseong 18449, Korea; Email: hyoon@ildong.com

Tae-im Kim – The Institute of Vision Research, Department of Ophthalmology, Severance Hospital, Yonsei University College of Medicine, Seoul 03722, Korea; Email: tikim@yuhs.ac

Wan Namkung – College of Pharmacy and Yonsei Institute of Pharmaceutical Sciences, Yonsei University, Incheon 21983, Korea; orcid.org/0000-0002-1480-7433; Email: wnamkung@yonsei.ac.kr

Authors

Bo Yi Kim – The Institute of Vision Research, Department of Ophthalmology, Severance Hospital, Yonsei University College of Medicine, Seoul 03722, Korea

Changmok Oh – Research Laboratories, ILDONG Pharmaceutical Co., Ltd., Hwaseong 18449, Korea

Dongkyu Jeon – College of Pharmacy and Yonsei Institute of Pharmaceutical Sciences, Yonsei University, Incheon 21983, Korea

Ikhyun Jun – The Institute of Vision Research, Department of Ophthalmology, Severance Hospital, Yonsei University College of Medicine, Seoul 03722, Korea

Ho K. Lee – College of Pharmacy and Yonsei Institute of Pharmaceutical Sciences, Yonsei University, Incheon 21983, Korea; orcid.org/0000-0003-1707-3217

Bo-Rahm Kim – The Institute of Vision Research, Department of Ophthalmology, Severance Hospital, Yonsei University College of Medicine, Seoul 03722, Korea

Jinhong Park – College of Pharmacy and Yonsei Institute of Pharmaceutical Sciences, Yonsei University, Incheon 21983, Korea

Kyoung Yul Seo – The Institute of Vision Research, Department of Ophthalmology, Severance Hospital, Yonsei University College of Medicine, Seoul 03722, Korea

Kyeong-A Kim – Research Laboratories, ILDONG Pharmaceutical Co., Ltd., Hwaseong 18449, Korea
Dami Lim – Research Laboratories, ILDONG Pharmaceutical Co., Ltd., Hwaseong 18449, Korea
Seolhee Lee – Research Laboratories, ILDONG Pharmaceutical Co., Ltd., Hwaseong 18449, Korea
Jooyun Lee – Research Laboratories, ILDONG Pharmaceutical Co., Ltd., Hwaseong 18449, Korea

Complete contact information is available at:

<https://pubs.acs.org/10.1021/acs.jmedchem.2c01382>

Author Contributions

B.Y.K., C.O., and D.J. contributed equally. The article was written through contributions of all authors. All authors have given approval to the final version of the article.

Funding

This work was supported by the National Research Foundation of Korea (NRF-2018R1A6A1A03023718, NRF-2020R1C1C1008332, and NRF-2021R1I1A1A01047951).

Notes

The authors declare no competing financial interest.

ACKNOWLEDGMENTS

The authors would like to thank Dr. Eung Kweon Kim of Saevit Eye Hospital at Goyang-si for his generous gift of CorE and ConjE cells.

ABBREVIATIONS

aq, aqueous; AUC, area under the curve; CFTR, cystic fibrosis transmembrane conductance regulator; CHO, Chinese hamster ovary; DCM, dichloromethane; DIPEA, *N,N*-diisopropylethylamine; DMF, dimethylformamide; EA, ethyl acetate; HBTU, 3-*bis*[(dimethylamino)methyl]iumyl]-3*H*-benzotriazol-1-oxide hexafluorophosphate; HRMS, high-resolution mass spectrometry; MeOH, methanol; MPLC, medium-pressure liquid chromatography; NMR, nuclear magnetic resonance; PBS, phosphate-buffered saline; PCR, polymerase chain reaction; PK, pharmacokinetics; r.t., room temperature; SAR, structure–activity relationship; SPR, structure–property relationship; TBAF, tetra-*n*-butylammonium fluoride; TBDMS, *tert*-butyldimethylsilyl chloride; TEA, triethylamine; TFA, Trifluoroacetic acid; THF, tetrahydrofuran; UPLC, ultra-performance liquid chromatography; YFP, yellow fluorescent protein

REFERENCES

- (1) Miljanović, B.; Dana, R.; Sullivan, D. A.; Schaumberg, D. A. Impact of dry eye syndrome on vision-related quality of life. *Am. J. Ophthalmol.* **2007**, *143*, 409–415.
- (2) Tatlipinar, S.; Akpek, E. K. Topical ciclosporin in the treatment of ocular surface disorders. *Br. J. Ophthalmol.* **2005**, *89*, 1363–1367.
- (3) The definition and classification of dry eye disease: report of the Definition and Classification Subcommittee of the International Dry Eye WorkShop (2007). *Ocul. Surf.* **2007**, *5*, 75–92.
- (4) Alves, M.; Fonseca, E. C.; Alves, M. F.; Malki, L. T.; Arruda, G. V.; Reinach, P. S.; Rocha, E. M. Dry eye disease treatment: a systematic review of published trials and a critical appraisal of therapeutic strategies. *Ocul. Surf.* **2013**, *11*, 181–192.
- (5) Donnenfeld, E. D.; Perry, H. D.; Nattis, A. S.; Rosenberg, E. D. Lifitegrast for the treatment of dry eye disease in adults. *Expert Opin. Pharmacother.* **2017**, *18*, 1517–1524.
- (6) Itoh, R.; Kawamoto, S.; Miyamoto, Y.; Kinoshita, S.; Okubo, K. Isolation and characterization of a Ca(2+)-activated chloride channel from human corneal epithelium. *Curr. Eye Res.* **2000**, *21*, 918–925.

- (7) Asbell, P. A.; Spiegel, S. Ophthalmologist perceptions regarding treatment of moderate-to-severe dry eye: results of a physician survey. *Eye Contact Lens* **2010**, *36*, 33–38.
- (8) Turner, H. C.; Bernstein, A.; Candia, O. A. Presence of CFTR in the conjunctival epithelium. *Curr. Eye Res.* **2002**, *24*, 182–187.
- (9) Al-Nakkash, L.; Reinach, P. S. Activation of a CFTR-mediated chloride current in a rabbit corneal epithelial cell line. *Invest. Ophthalmol. Vis. Sci.* **2001**, *42*, 2364–2370.
- (10) Yu, D.; Thelin, W. R.; Rogers, T. D.; Stutts, M. J.; Randell, S. H.; Grubb, B. R.; Boucher, R. C. Regional differences in rat conjunctival ion transport activities. *Am. J. Physiol. Cell Physiol.* **2012**, *303*, C767–C780.
- (11) Morkeberg, J. C.; Edmund, C.; Prause, J. U.; Lanng, S.; Koch, C.; Michaelsen, K. F. Ocular findings in cystic fibrosis patients receiving vitamin A supplementation. *Graefes Arch. Clin. Exp. Ophthalmol.* **1995**, *233*, 709–713.
- (12) Mrugacz, M.; Minorowska, A.; Bakunowicz-Lazarczyk, A.; Zywalewska, N. [Dry eye syndrome in children with cystic fibrosis]. *Med. Wieku Rozwoj.* **2004**, *8*, 865–870.
- (13) Boyer, J.; Johnson, M. R.; Ansed, J.; Donn, K.; Boucher, R.; Thelin, W. P. 321, a novel long-acting epithelial Sodium Channel (ENaC) blocker for the treatment of dry eye disease. *Investig. Ophthalmol. Vis. Sci.* **2013**, *54*, 957.
- (14) Flores, A. M.; Casey, S. D.; Felix, C. M.; Phuan, P. W.; Verkman, A. S.; Levin, M. H. Small-molecule CFTR activators increase tear secretion and prevent experimental dry eye disease. *FASEB J.* **2016**, *30*, 1789–1797.
- (15) Chen, X.; Lee, S.; Zhang, T.; Duan, T.; Pasricha, N. D.; Schallhorn, J. M.; Levin, M. H.; Koprivica, V.; Verkman, A. S. Nanomolar Potency Aminophenyltriazine CFTR Activator Reverses Corneal Epithelial Injury in a Mouse Model of Dry Eye. *J. Ocul. Pharmacol. Ther.* **2020**, *36*, 147–153.
- (16) Pasricha, N. D.; Smith, A. J.; Levin, M. H.; Schallhorn, J. M.; Verkman, A. S. Ocular Surface Potential Difference Measured in Human Subjects to Study Ocular Surface Ion Transport. *Transl. Vis. Sci. Technol.* **2020**, *9*, 20.
- (17) Chauhan, S. K.; El Annan, J.; Ecoiffier, T.; Goyal, S.; Zhang, Q.; Saban, D. R.; Dana, R. Autoimmunity in dry eye is due to resistance of Th17 to Treg suppression. *J. Immunol.* **2009**, *182*, 1247–1252.
- (18) Lee, H. K.; Park, J.; Kim, B.-R.; Jun, I.; Kim, T.-I.; Namkung, W. Isorhamnetin Ameliorates Dry Eye Disease via CFTR Activation in Mice. *Int. J. Mol. Sci.* **2021**, *22*, 3954.
- (19) Ma, T.; Thiagarajah, J. R.; Yang, H.; Sonawane, N. D.; Folli, C.; Galletta, L. J.; Verkman, A. S. Thiazolidinone CFTR inhibitor identified by high-throughput screening blocks cholera toxin-induced intestinal fluid secretion. *J. Clin. Invest.* **2002**, *110*, 1651–1658.
- (20) Stern, M. E.; Gao, J.; Schwalb, T. A.; Ngo, M.; Tieu, D. D.; Chan, C. C.; Reis, B. L.; Whitcup, S. M.; Thompson, D.; Smith, J. A. Conjunctival T-cell subpopulations in Sjogren's and non-Sjogren's patients with dry eye. *Invest. Ophthalmol. Vis. Sci.* **2002**, *43*, 2609–2614.
- (21) Niederkorn, J. Y.; Stern, M. E.; Pflugfelder, S. C.; De Paiva, C. S.; Corrales, R. M.; Gao, J.; Siemasko, K. Desiccating stress induces T cell-mediated Sjogren's Syndrome-like lacrimal keratoconjunctivitis. *J. Immunol.* **2006**, *176*, 3950–3957.
- (22) Jeon, D.; Jun, I.; Lee, H. K.; Park, J.; Kim, B.-R.; Ryu, K.; Yoon, H.; Kim, T.-i.; Namkung, W. Novel CFTR Activator Cact-3 Ameliorates Ocular Surface Dysfunctions in Scopolamine-Induced Dry Eye Mice. *Int. J. Mol. Sci.* **2022**, *23*, 5206.
- (23) Shirasaki, Y. Molecular design for enhancement of ocular penetration. *J. Pharmaceut. Sci.* **2008**, *97*, 2462–2496.
- (24) Gukasyan, H. J.; Hailu, S.; Karami, T. K.; Graham, R. Ocular biopharmaceutics: impact of modeling and simulation on topical ophthalmic formulation development. *Drug Discovery Today* **2019**, *24*, 1587–1597.
- (25) Liu, F.; Zhang, Z.; Levit, A.; Levring, J.; Touhara, K. K.; Shoichet, B. K.; Chen, J. Structural identification of a hotspot on CFTR for potentiation. *Science* **2019**, *364*, 1184–1188.
- (26) Meanwell, N. A. Fluorine and fluorinated motifs in the design and application of bioisosteres for drug design. *J. Med. Chem.* **2018**, *61*, 5822–5880.

(27) Ishikawa, M.; Hashimoto, Y. Improvement in aqueous solubility in small molecule drug discovery programs by disruption of molecular planarity and symmetry. *J. Med. Chem.* **2011**, *54*, 1539–1554.

(28) Seo, Y.; Lee, H. K.; Park, J.; Jeon, D.-k.; Jo, S.; Jo, M.; Namkung, W. Ani9, a novel potent small-molecule ANO1 inhibitor with negligible effect on ANO2. *PLoS One* **2016**, *11*, No. e0155771.

(29) Jeon, D.; Ryu, K.; Jo, S.; Kim, I.; Namkung, W. VI-116, A Novel Potent Inhibitor of VRAC with Minimal Effect on ANO1. *Int. J. Mol. Sci.* **2022**, *23*, 5168.

(30) *Schrödinger Release 2022-2*; Maestro, Schrödinger LLC: New York, NY, 2021.

(31) Bron, A. J.; Evans, V. E.; Smith, J. A. Grading of corneal and conjunctival staining in the context of other dry eye tests. *Cornea* **2003**, *22*, 640–650.